Jarkko Peuron
Master's thesis
Instructor: Tuomas Lappi

University of Jyväskylä
Department of Physics
September 5, 2014

Determination of the non-abelian Debye screening mass using classical chromodynamics

UNIVERSITY OF JYVÄSKYLÄ

Contents

Abstract

In this work we study the gluon Debye screening mass and its dependence on time and occupation number distribution using classical chromodynamics in two spatial dimensions. We also study the characteristic momentum scale and occupation number distributions. We determine the gluon Debye screening mass by performing linear fits into the gluon dispersion relation in the low momentum regime. We compare the result to the one obtained using a formula derived from thermal field theory.

We start by quickly reviewing the heavy-ion physics context for this work. Then we quickly recap the classical Yang-Mills theory in the continuum and on the lattice.

We will go through a Fourier accelerated Coulomb gauge fixing procedure in detail in the continuum theory and on the lattice. This will be an essential part of this work, as some observables we use are meaningful only in the Coulomb gauge.

Then we introduce the gauge invariant and gauge dependent observables and the initial conditions used. In this work we find evidence for the existence of a non-zero Debye screening mass at high occupation numbers and late dimensionless times. We observe that the Debye mass gets bigger at higher occupation numbers as expected from thermal field theory.

According to the thermal field theory the gluon Debye mass is also time dependent through its occupation number distribution dependence. Due to low statistics we cannot draw any firm conclusions about the time dependence of the Debye screening mass.

Tiivistelmä

Tässä työssä tutkitaan gluonin Debye-massaa, ja sen aika- ja miehityslukudistribuutioriippuvuutta käyttäen klassista väridynamiikkaa kahdessa paikkaulottuvuudessa. Työssä tutkitaan myös ominaista liikemääräskaalaa ja miehityslukudistribuutioita. Gluonin Debye-massa määritetään sovittamalla suora gluonien dispersiorelaatioon pienellä liikemäärällä. Tuloksia verrataan termisestä kenttäteoriasta johdetun kaavan ennusteisiin.

Aluksi tutustutaan raskasionifysiikkaan liittyvään viitekehykseen. Tämän jälkeen kerrataan nopeasti klassinen Yang-Mills teoria jatkumossa ja hilalla.

Käydään läpi Fourier kiihdytetty Coulombin mitan kiinnitysmenetelmä yksityiskohtaisesti jatkumossa ja hilalla. Tämä tulee olemaan oleellinen osa työtä, koska jotkut käytetyt observaabelit ovat mielekkäitä ainoastaan Coulombin mitassa.

Tämän jälkeen esitellään työssä käytetyt mittariippumattomat ja mittariippuvat observaabelit ja käytetyt alkuehdot. Löydetään viitteitä gluonin nollasta poikkeavan Debye-massan olemassaolosta suurilla miehitysluvilla ja myöhäisillä dimensiottomilla ajoilla. Havaitaan, että gluonin Debye-massa kasvaa suuremmilla miehitysluvuilla, kuten termisestä kenttäteoriasta voisikin odottaa.

Termisen kenttäteorian mukaan gluonin Debye-massa riippuu myös ajasta miehityslukudistribuutionsa aikariippuvuuden kautta. Alhaisen statistiikan takia ei voida kuitenkaan vetää varmoja johtopäätöksiä Debye-massan aikariippuvuudesta.

1 Introduction

The goal of heavy-ion physics is to produce Quark-Gluon Plasma (QGP), a deconfined state of matter consisting of free quarks and gluons, whose existence is predicted by Quantum ChromoDynamics (QCD) [1][2][3][4]. Currently the properties of the quark-gluon plasma are studied at the Relativistic Heavy-Ion Collider (RHIC) [5] [6] [7][8] at Brookhaven National Laboratory (BNL) and the large hadron collider (LHC) at CERN [9][10][11] [12][13].

The space-time picture of a relativistic heavy-ion collision (which can be seen in the figure 1.1), can be divided in roughly three parts. After the collision the formed matter is in a pre-equilibrium state, which is sometimes also known as the glasma phase. The matter then isotropizes and eventually thermalizes. At this point we can call the matter QGP, as it is in thermal equilibrium. The QGP undergoes rapid expansion and cooling. In this phase hydrodynamics (first viscous and finally ideal) is applicable. As the system cools partons start to form hadrons, which interact and form a hadron gas. (When we have only hadron gas left, the system enters the hadron gas phase.) Eventually, due to further expansion and cooling, interactions between hadrons cease and the system drops out of equilibrium, which is called the freeze out.

The experimental results show apparently fast thermalization according to the successful hydrodynamical description of the quark-gluon plasma [5][7][9] [14][15] [16]. The observed thermalization time of the order of one fermi[7] poses a major challenge for theory, and there is still no consensus how isotropization and thermalization of the QGP happens. In this work we will solve the classical Yang-Mills equations of motion numerically on the lattice, which is mainly relevant for the pre-equilibrium phase in the framework of heavy-ion physics.

From the theory side our understanding of ultra-relativistic heavy-ion collisions relies mostly on QCD in the weak coupling limit. Also alternative approaches to thermalization have emerged recently, namely holographic ther-

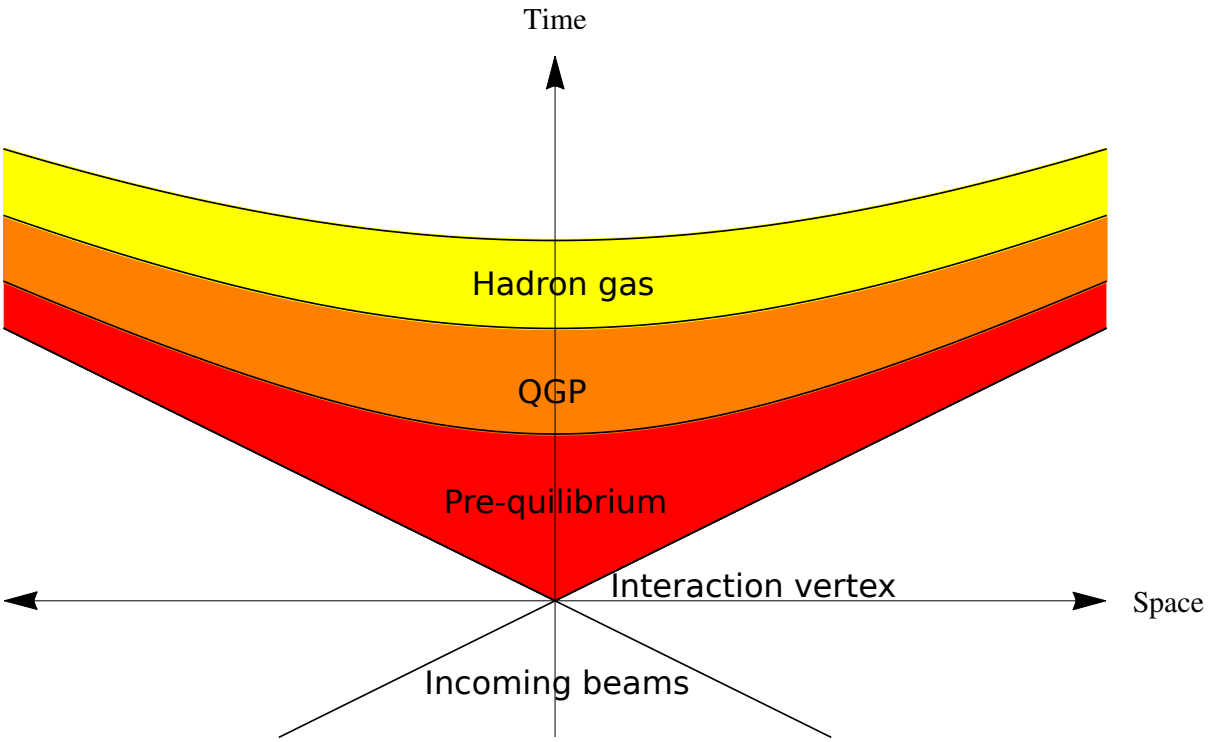

Figure 1.1: Schematic space-time picture of a heavy ion collision. The hyperbolae represent different proper time $\tau = \sqrt{t^2 - z^2} = \text{constant}$ curves. Different phases have been marked with different colors.

malization scenarios, which rely on gauge-string dualities in supersymmetric Yang-Mills theories[17][18]. In this framework one can study strongly coupled non-abelian plasma, which is qualitatively different from weakly coupled one [17]. The strong coupling results are derived for $\mathcal{N} = 4$ super Yang-Mills plasma, which is not strictly speaking the same as strongly coupled QCD plasma. However, these calculations still provide us some insight about the strongly coupled non-Abelian plasma. The question whether the QGP really is strongly or weakly coupled is beyond the scope of this work.

Starting from QCD, a heavy-ion collision can be described using the Color Glass Condensate (CGC) framework, which is an effective theory of QCD in the high energy weak coupling regime [19] (for more information on CGC see for example [20][21]). In the weak coupling framework a collision of large nuclei creates gluon states of very high occupancy [22]. In this regime we can treat the gluons as classical color fields [23], and therefore the dynamics is essentially classical and can be studied using classical statistical lattice gauge theory [22]. Lattice gauge theory is necessary here, because the classical Yang-

Mills equations of motion are highly non-linear, and therefore extremely hard to solve analytically (without any approximations). The equations of motion are best solved using Wilson's lattice formulation [24] to preserve gauge invariance, which will be lost in a naive discretization.

Weakly coupled non-abelian plasmas are known to exhibit plasma instabilities. Perhaps the best known instabilities are the chromo-Weibel instability [25][26] and the Nielsen-Olesen instability [27]. There are hints that strongly coupled plasmas may exhibit similar behaviour [28]. Plasma instabilities have also been proposed to be one possible mechanism driving the plasma towards isotropization [29]. In this work we study the gluon Debye screening mass instead of plasma instabilities. Debye screening in electromagnetic plasma suppresses the Coulomb potential between two point charges exponentially. The scale of this exponential suppression is given by the Debye screening length, which is also the characteristic length scale of the plasma. The inverse of the Debye sceening length is the Debye mass, which in the case of electromagnetic plasma is the photon effective mass. In the non-abelian plasma there is a similar screening for the color electric fields, which gives the gluon effective mass. The connection between the Debye screening mass and plasma instabilities is that for the non-abelian plasma instabilities the growth rate of the plasma instabilities determined by the plasmon mass (which in our case is the same as the gluon Debye mass) [30].

Using classical statistical lattice simulations we can actually calculate the plasmon mass assosiated to these plasma oscillations by studying the gluon dispersion relation, from which the plasmon mass is obtained at its value at zero momentum [30]. The plasmon mass is also calculable from thermal field theory. In thermal field theory one calculates the needed propagator corrections in thermal background and then finally gets the plasmon mass as the pole of the corrected propagator [31]. In this work we will compare our results obtained from the gluon dispersion relation with ones we get by utilizing a prescription derived from thermal field theory.

All simulations in this work have been done in two spatial dimensions. The implementation is particularly straightforward: we simply shrink the spatial extent of our lattice to one point in the longitudinal direction. This will simplify our numerical work in various ways. First it allows us to use significantly smaller lattice sizes (as we have eliminated one entire dimension), but yet it still allows us to study qualitatively happens in the transverse plane in an ultra relativistic heavy-ion collision. Thus it is a very good starting point. In the future we want to study these effects and plasma instabilities in the three dimensional case, and thus our code is written for three dimensions. This allows us to easily extend our work without needing to write a new code

for it. In a fully three dimensional simulation we can also take into account the characteristic asymmetry in the initial conditions. In a ultra relativistic heavy-ion collision the initial momentum distribution of the outgoing particles is highly anisotropic - the particles created in the collision have very high transverse momenta, but relatively low longitudinal momenta. Working in two dimensions also greatly simplifies the numerical work, because the Coulomb gauge fixing is considerably harder when the momenta in the longitudinal direction are close to zero.

The initial momentum distribution we used in our simulation is essentially a Gaussian distribution multiplied by the momentum. There is no physical reason behind this, but it creates a very clear typical momentum scale (which we will refer to as Δ), and it allows us to effectively cross-check our results, because Berges et al. have used similar initial states in their publications [32][33][34].

Kinetic theory might also provide some insight for our lattice approach, because these two have an overlapping range of validity. The classical statistical approach is valid at high occupation numbers, i.e. $n(p) \gg 1$. Kinetic theory, on the other hand, is valid until $n(p) \ll 1/\alpha_s$ [22]. It has also been argued that kinetic theory and classical field theory are actually equivalent when the typical occupation numbers are large [35] [36]. And indeed it has been shown that they can yield quantitatively similar results at least for the UV cascade [37] [38]. We will not use kinetic theory in this work, but it would be interesting to see whether it is in agreement with our results in the future.

2 Theoretical background

2.1 Yang-Mills theory

The Yang-Mills theory [39] is defined by the Lagrangian

$$\mathcal{L} = -\frac{1}{2}\mathrm{Tr}\left(F_{\mu\nu}F^{\mu\nu}\right), \tag{2.1.1}$$

where $F^{\mu\nu} = \partial^\mu A^\nu - \partial^\nu A^\mu + ig\left[A^\mu, A^\nu\right]$ is the non-abelian field strength tensor, A_μ is the gluon field and the trace is taken over the $SU(N)$ color space. A_μ and $F_{\mu\nu}$ are N^2 hermitian traceless matrices in the color space. Using the Euler-Lagrange equation one can obtain the equations of motion of the theory without external sources in the fundamental representation of $SU(N)$:

$$\left[D^\mu, F_{\mu\nu}\right] = 0, \tag{2.1.2}$$

where D^μ is the gauge covariant derivative defined as $D^\mu = \partial^\mu + igA^\mu$. By choosing $\nu = 0$ we get the non-abelian Gauss's law

$$[D_i, E_i] = 0, \tag{2.1.3}$$

which is a non-dynamical constraint (as it contains no time derivatives). However it is an important sanity check for our simulation, and it also needs to be taken into account with our initial state.

The Lie-algebra valued color electric field appearing in the equation (2.1.3) is defined as

$$E_i = F_{i0}, \tag{2.1.4}$$

and the color magnetic field is defined as

$$B_i = \frac{-\varepsilon_{ijk}}{2}F^{jk}. \tag{2.1.5}$$

By performing a Legendre transformation on the Yang-Mills Lagrangian (2.1.1) one obtains the Hamiltonian density correspoding to (2.1.1)

$$\mathcal{H} = \mathrm{Tr}\left(E_i^2 + B_i^2\right), \tag{2.1.6}$$

which is given in temporal gauge. Gauge fixing is essential, because while performing the Legendre transformation we observe that the temporal component of the gluon field has no canonical momentum and the only way to circumvent this problem is to eliminate it by fixing the gauge. Later on we will be interested in the electric energy, magnetic energy, and total energy of our system, and these are given by integrating equation (2.1.6) over the whole space.

2.2 Gauge fixing and the Gribov ambiguity

In gauge theories there are always unphysical degrees of freedom which give us ability to perform gauge transformations on our fields without changing the real physical fields. If one field configuration can be obtained from the other by performing a gauge transformation these field configurations are physically equivalent, and they are said to belong to same gauge orbit. In gauge fixing procedure, we want to (in the ideal case) to choose only one representative from each gauge orbit. This is especially important when evaluating path integrals to eliminate double counting. In the classical field theory this is not a concern, but gauge fixing can simplify our equations considerably. Gauge fixing is also, of course, important when we are interested in gauge dependent quantities. However, these are not observables, as those are always gauge invariant.

In this work we will employ two gauges. The temporal gauge, which eliminates the temporal component of the gluon field, and the Coulomb gauge, which eliminates the divergence of the gluon field. Before going into details one should also note that gauge fixing in non-abelian gauge theory is considerably harder than in abelian gauge theory. It can also be shown that in the non-abelian gauge theory the Coulomb gauge condition does not uniquely determine the gluon field, i.e. we have many field configurations which satisfy the Coulomb gauge condition. This is known as the Gribov ambiguity [40].

The temporal gauge, which we will use in this work, is particularly simple to fix. It is given by condition

$$A_0 = 0. \tag{2.2.1}$$

This is also easy to implement on the lattice. The Coulomb gauge is fixed by requiring the divergence of the gluon field to vanish

$$\boldsymbol{\nabla} \cdot \boldsymbol{A} = 0. \tag{2.2.2}$$

However, there is an alternative gauge condition for the Coulomb gauge. It can be shown, that Coulomb gauge is the gauge that minimizes the integral of $\boldsymbol{A}^2$ over the whole space [41]. This is easy to see in the classical electrodynamics, where we can decompose the integral of the vector potential squared as

$$\begin{aligned}\int \boldsymbol{A}^2 \mathrm{d}^3x = \frac{1}{4\pi}\int \mathrm{d}^3x\mathrm{d}^3x' \frac{(\boldsymbol{\nabla}\times\boldsymbol{A}(x))\cdot\left(\boldsymbol{\nabla}'\times\boldsymbol{A}\left(x'\right)\right)}{|\boldsymbol{x}-\boldsymbol{x'}|} \\ + \frac{1}{4\pi}\int \mathrm{d}^3x\mathrm{d}^3x' \frac{(\boldsymbol{\nabla}\cdot\boldsymbol{A}(x))\left(\boldsymbol{\nabla}'\cdot\boldsymbol{A}\left(x'\right)\right)}{|\boldsymbol{x}-\boldsymbol{x'}|},\end{aligned} \tag{2.2.3}$$

where we have neglected the surface terms. This expression is derived in appendix B. The curl of the vector potential is gauge invariant, so clearly the integral is minimized when the divergence of the vector potential is zero. Numerically it is much easier to minimize this than to keep track of the divergence of $\boldsymbol{A}$ on every point in space, as we can rather simply minimize the integral (2.2.3).

As we want to consider scenarios relevant for heavy-ion physics, we want to use anisotropic momentum distributions for gluons. We are especially interested in an asymmetric situation, in which the momentum distribution is symmetric in the transverse plane, but resembles a delta function in the longitudinal direction. The momentum anisotropy makes gauge fixing considerably harder, because our gauge condition does not constrain the gluon field in the longitudinal direction very much. This is why we want to find as powerful a gauge fixing algorithm as possible.

Next we find a way to minimize the integral (2.2.3). Here we follow very closely reference [42]. First, consider the simple case of classical electrodynamics. The gauge transformation for the magnetic vector potential is

$$A_\mu \to A_\mu - \partial_\mu \chi. \tag{2.2.4}$$

Now we want to minimize the integral (2.2.3). Let us choose $\chi = \alpha\boldsymbol{\nabla}\cdot\boldsymbol{A}$, We do a gauge transformation on the equation (2.2.3) and integrate the term proportional to α by parts. We get

$$\int \boldsymbol{A}^2\mathrm{d}^3x \to \int \mathrm{d}^3x\left(\boldsymbol{A}^2 - 2\alpha\left(\partial_i A^i\right)^2 + \alpha^2\partial_j\partial_i A^i\partial^j\partial_k A^k\right). \tag{2.2.5}$$

From this expression we can see that choosing α sufficiently small, we can minimize the integral (2.2.3) by an iterative procedure. However, we will soon see that this algorithm is not very efficient in minimizing the integral (2.2.3).

Now consider the n$^{\text{th}}$ step of the previous procedure

$$\partial_i A^{i(n)} = \partial_i A^{i(n-1)} + \alpha \partial^2 \partial_j A^{j(n-1)}. \tag{2.2.6}$$

Now we decompose $\boldsymbol{A}$ into Fourier components, and denote them by tilde. We get

$$\boldsymbol{\partial} \cdot \tilde{\boldsymbol{A}}^{(n)} = \left(\boldsymbol{\partial} \cdot \tilde{\boldsymbol{A}}^{(0)}\right) \left(1 - \alpha k^2\right)^n \approx \left(\boldsymbol{\partial} \cdot \tilde{\boldsymbol{A}}^{(0)}\right) \exp\left(-\alpha k^2 n\right), \tag{2.2.7}$$

where the last approximation was made in the limit when n becomes large. We have denoted the eigenvalues of the $\boldsymbol{\partial}^2$ by k^2. From the equation (2.2.7) we can see that the convergence of each Fourier mode depends on the wavenumber and that longer wavelengths converge slower than short ones. We also observe that the mode corresponding to zero will never converge, but this is not an issue, because the gauge transformation corresponding to the zero mode is present in the whole space, and therefore corresponds to a global gauge transformation.

We can see from the equation (2.2.7) that stability requires $\alpha < \dfrac{1}{k^2_{max}}$, where we have denoted the maximum eigenvalue of $\boldsymbol{\partial}^2$ by k^2_{max}. The existence of maximum (or minimum) eigenvalue of $\boldsymbol{\partial}^2$ will not be a problem in this work, because the lattice discretization will regulate our theory both in the ultraviolet and in the infrared. Now we observe that the time taken for the smallest eigenvalue of $\boldsymbol{\partial}^2$ to converge is

$$t_{min} \propto \frac{k^2_{max}}{k^2_{min}}. \tag{2.2.8}$$

If we perform the lattice discretisation with hypercubic lattice of length L, for the minimum eigenvalue of $\boldsymbol{\partial}^2$ we have $k^2_{min} \propto 1/L^2$. The time taken to perform the rest of the algorithm (the gauge transformation) is proportional to V. Thus the time needed to fix the Coulomb gauge using this algorithm is proportional to $V^{5/3}$ in three dimensions and V^2 in two dimensions. This is known as critical slowing down, as the gauge fixing becomes considerably harder when the size of the lattice increases.

Fortunately, we can do better than this. Previously the convergence was controlled by the long wavelength modes. Using a Fourier transform and by adjusting the step size in the momentum space, we can actually make all momentum components converge at the same rate. This is achieved by choosing the step size in the momentum space as

$$\alpha(p) = \alpha \frac{p^2_{max}}{p^2}. \tag{2.2.9}$$

With Fourier acceleration, the gauge transformation done at each iteration becomes

$$\partial_\mu \chi = \hat{F}^{-1} \alpha \frac{p_{max}^2}{p^2} \hat{F} \partial_\mu \partial_i A^i(x), \tag{2.2.10}$$

where $\hat{F}$ denotes a Fourier transform (Fast Fourier Transform (FFT) in the discretized case). Execution time of this algoritm grows as $V \ln(V)$, as the cost of FFT is proportional to $V \ln(V)$, and the time taken to execute of the rest of the algorithm is proportional to V.

It is also easy to show that the Coulomb gauge can be fixed with only one iteration. Starting from the equation (2.2.4) we impose the condition that the divergence of the transformed field vanishes. We get an equation for χ

$$\boldsymbol{\nabla} \cdot \boldsymbol{A} - \boldsymbol{\nabla}^2 \chi = 0. \tag{2.2.11}$$

This has a formal solution

$$\chi = \frac{\boldsymbol{\nabla} \cdot \boldsymbol{A}}{\boldsymbol{\nabla}^2}. \tag{2.2.12}$$

Equation (2.2.11) is actually a Poisson equation for χ with a source term of $\boldsymbol{\nabla} \cdot \boldsymbol{A}$. A standard technique to solve equations of this type is by doing a Fourier transform (which clarifies the role of the inverse of $\boldsymbol{\nabla}^2$ in equation (2.2.12)). In position space the solution becomes

$$\chi = \hat{F}^{-1} \frac{1}{k^2} \hat{F} \boldsymbol{\nabla} \cdot \boldsymbol{A}. \tag{2.2.13}$$

This corresponds to equation (2.2.10) with choice $\alpha = 1/k_{\text{max}}^2$, which in the continuous case cancels the singularity associated with k_{max}^2.

The gauge fixing procedure on the lattice is quite similar to the continuum procedure, but there we will change the degrees of freedom of our theory to the appropriate ones in order to preserve exact gauge invariance. The lattice gauge fixing procedure will be discussed in detail in section 3.2.

One should also note that the gauge fixing procedure becomes more complicated when dealing with a non-Abelian theory. In abelian theory we were dealing with the eigenvalues of the operator $\boldsymbol{\partial}^2$, but in the non-Abelian theory the relevant operator becomes $\boldsymbol{\partial} \cdot \boldsymbol{D}$, as the gauge transformation becomes $A_\mu \to A_\mu - D_\mu \chi$. This means that the eigenvalues are no longer independent of the field. Fortunately this does not turn out to be as big of an issue as one might think, but it does have an impact on the efficiency of our algorithm [42].

2.3 Debye screening mass

Fundamental properties of elementary particles can be modified by interactions. This effect is present when particles propagate trough a medium, with which they interact. Particles may, for example, acquire an effective mass, which is different from the one measured in the vacuum [31]. Perhaps the best known example of this is the screening of the electric field of a point charge in a static thermal background in QED.

In the classical electrodynamics the potential between two point charges is given by the Coulomb potential. However, in QED we can calculate the potential between the two point charges in static thermal background. We find out that the Coulomb potential turns into the Yukawa potential

$$V(r) \sim \frac{\exp\left(-r/r_D\right)}{r}, \tag{2.3.1}$$

i.e. the electric field is screened with a characteristic length scale r_D [31]. The inverse of r_D is the Debye screening mass m_D, which is the effective mass of the photon in a static thermal background.

We are interested in whether a similar behaviour can be observed in non-abelian plasma (i.e. plasma in which the mediators of the interaction interact also with each other, unlike in abelian plasma). It turns out that color electric fields indeed get screened by interactions in thermal plasma. The value of the screening mass can be calculated from thermal field theory [31].

In this work we will extract the value of the gluon Debye mass from gluon dispersion relation, and then compare it to the one which can be obtained from the thermal field theory.

3 Lattice formulation

3.1 Lattice formulation of SU(N) Yang-Mills theory

For a more thorough discussion on the lattice formulation of non-abelian gauge theory see e.g. [43] and [44]. In order to preserve gauge invariance in local SU(N) gauge transformations we change the degrees of freedom of our theory from Lie algebra ($\mathfrak{SU}(N)$) valued gauge fields A_μ to Lie group valued link matrices U, defined as

$$U_{x,\mu} = \exp\Big(iga_\mu A_\mu(x)\Big), \tag{3.1.1}$$

which is a discretized version of the Schwinger line integral. The calculation of matrix exponentials in $\mathfrak{SU}(2)$ is explained in detail in the appendix C. The physical interpretation for this is that a fermion wavefunction picks up a phase factor which is given by the Schwinger line integral when moving in the presence of a gauge field [44]. In a local SU(N) gauge transformation the link matrix transforms as $U_{x,\mu} \to V(x)U_{x,\mu}V^\dagger(x+\mu)$, where the notation $x+\mu = x + a_\mu\hat{\mu}$. Here a_μ stands for lattice spacing in the μ-direction. $a_\mu = a_s$ when $\mu = 1,2,3$ and $a_\mu = a_t$ when $\mu = 0$. One should also remember that we are using periodic boundary conditions. Using this we can build gauge invariant observables by forming closed loops on the lattice with link matrices, which are called Wilson loops, or plaquettes in the simplest 1×1 loop case, and by taking the trace. The plaquette is proportional to the field strength tensor in the continuum limit

$$U_{x,\mu\nu} \equiv U_{x,\mu}U_{x+\mu,\nu}U^\dagger_{x+\nu,\mu}U^\dagger_{x,\nu} \approx \exp\Big(iga_\mu a_\nu F_{\mu\nu}\Big), \tag{3.1.2}$$

as some algebra shows. Using this piece of information we can establish a connection between the lattice quantities and the continuum quantities. By

expanding to the lowest non-trivial order in lattice spacing we find that the right hand side of the following expressions converge to the continuum expression of the left hand side when taking the limit $a \to 0$

$$E_i^a(x) = \frac{2}{a_s a_t g}\mathfrak{Im}\mathrm{Tr}(t^a U_{x,i0}) \tag{3.1.3}$$

$$B_i^a(x) = -\frac{\varepsilon_{ijk}}{a_s^2 g}\mathfrak{Im}\mathrm{Tr}\left(t^a U_{x,jk}\right) \tag{3.1.4}$$

$$F_{\mu\nu}^a(x) = \frac{2}{a_\mu a_\nu g}\mathfrak{Im}\mathrm{Tr}\left(t^a U_{x,\mu\nu}\right). \tag{3.1.5}$$

$$A_\mu^a(x) = \frac{2}{a_\mu g}\mathfrak{Im}\mathrm{Tr}\left(t^a U_{x,\mu}\right). \tag{3.1.6}$$

The t^a are generators of $SU(N)$, normalised as $\mathrm{Tr}\left(t^a t^b\right) = \frac{1}{2}\delta^{ab}$, $a = 1, 2, \ldots N^2 - 1$. If $N = 2$ these are Pauli matrices divided by two, and if $N = 3$ they are Gell-Mann matrices divided by two.

It is then not hard to show that in 3+1 dimensional Minkowski space-time the Yang-Mills action (2.1.1) is reproduced by the following Wilson action [24] as the lattice spacing goes to zero:

$$\begin{aligned}\mathcal{S} = &-\beta_0 \sum_x \sum_i \left(\frac{1}{2N}(\mathrm{Tr}(U_{x,0i}) + \mathrm{Tr}(U_{x,0i}^\dagger)) - 1\right) \\ &+ \beta_s \sum_x \sum_{i<j} \left(\frac{1}{2N}(\mathrm{Tr}(U_{x,ij}) + \mathrm{Tr}(U_{x,ij}^\dagger)) - 1\right).\end{aligned} \tag{3.1.7}$$

Varying this with respect to spatial links gives the equations of motion

$$\begin{aligned}E_j^b(t,x) = E_j^b(t - a_t, x) - \frac{2}{\gamma^2 a_s a_t g}\sum_k \Bigg(&\mathfrak{Im}\mathrm{Tr}\left(t^b U_{x,k} U_{x+k,j} U_{x+j,k}^\dagger U_{x,j}^\dagger\right) \\ &- \mathfrak{Im}\mathrm{Tr}\left(t^b U_{x,j} U_{x+j-k,k}^\dagger U_{x-k,j}^\dagger U_{x-k,k}\right)\Bigg),\end{aligned} \tag{3.1.8}$$

where temporal gauge has been adopted. This sets temporal links to unity. It is straightforward to verify that these equations of motion are also gauge invariant by writing them into matrix form. This is also more convenient to solve using a

computer, since we do not have to solve essentially the same equation many times. The matrix form is

$$E_j(t,x) = E_j(t-a_t,x) + \frac{a_t}{2ia_s^3 g}\sum_k \Bigg(U_{x,jk} - U_{x,jk}^\dagger - \frac{\mathbb{1}}{N}\mathrm{Tr}\left(U_{x,jk} - U_{x,jk}^\dagger\right) \quad (3.1.9)$$
$$+ U_{x,j}U_{x-k+j,k}^\dagger U_{x,-k,j}^\dagger U_{x-k,k} - \left(U_{x,j}U_{x-k+j,k}^\dagger U_{x,-k,j}^\dagger U_{x-k,k}\right)^\dagger$$
$$- \frac{\mathbb{1}}{N}\mathrm{Tr}\left(U_{x,j}U_{x-k+j,k}^\dagger U_{x,-k,j}U_{x-k,k} - \left(U_{x,j}U_{x-k+j,k}^\dagger U_{x,-k,j}^\dagger U_{x-k,k}\right)^\dagger\right)\Bigg),$$

which can be found by writing the traces in terms of components, and the imaginary part with the help of the matrix and its hermitean conjugate. Finally one multiplies by t^b and uses a Fierz identity. Varying the action with respect to temporal links gives the discrete analogy of the Gauss constraint (2.1.3)

$$\sum_j \left(E_j(x) - U_{x-j,j}^\dagger E_j(x-j)U_{x-j,j}\right) = 0. \quad (3.1.10)$$

We evolve our system forward in time using an algorithm similar to ref. [33], proceeding as follows:

1. Using the equation (3.1.9) evolve electric fields to next time-step.
2. Using the definition of the color electric field on the lattice (3.1.3) calculate the temporal plaquette.
3. Using the definition of the temporal plaquette in the temporal gauge solve the link at the next timestep.

In order to simplify the numerical work we adopt SU(2) gauge group for the simulations. The biggest differences between SU(2) and SU(3) simulations would occur in step 2, where there is no trivial way to calculate the temporal plaquette for SU(3), but for SU(2) this turns out to be rather straightforward, because calculating the exponential of a $\mathfrak{SU}(2)$ matrix is rather easy, but for a $\mathfrak{SU}(3)$ this cannot be done analytically.

We do not expect this simplification to affect our results qualitatively. Studies have been done using both gauge groups and the results have turned out to be qualitatively similar in the classical statistical gauge theory [33] and also in the kinetic theory [45].

Now let us take a closer look at the steps performed when calculating the time evolution of our system. When we know the links, step one is rather

straightforward to perform. In step two, we use the fact that every SU(2) matrix can be decomposed in the following way

$$U_{x,i0} = c_0 \mathbb{1} + 2ic^a t^a, \tag{3.1.11}$$

where $1 = \sqrt{c_0^2 + c_a c_a}$. This is fairly easy to prove by starting from the form of a general 2 by 2 SU(2) matrix $U = \begin{pmatrix} \alpha & -\bar{\beta} \\ \beta & \bar{\alpha} \end{pmatrix}$, where $\sqrt{|\alpha|^2 + |\beta|^2} = 1$. Now we can easily see that equation (3.1.11) gives us matrices of this form and the constraint $1 = \sqrt{c_0^2 + c_a c_a}$ guarantees that the determinant is equal to one.

Using the definition of the color electric field (3.1.3), and plugging in the decomposition (3.1.11) for the temporal plaquette, we obtain $c_a = \frac{a_s a_t g}{2} E_a$. So we can easily solve for the temporal plaquette

$$U_{x,i0} = \sqrt{1 - \left(\frac{a_s a_t g}{2} E_a\right)^2}\mathbb{1} + i a_s a_t g E^a t^a. \tag{3.1.12}$$

After this solving the link matrix for the next time-step from the definition of the temporal plaquette in the temporal gauge is trivial: $U_{x+t,i} = U^\dagger_{x,i0} U_{x,i}$.

In order to verify that our simulation works correctly we have to verify that energy is conserved. The Hamiltonian corresponds to the total energy of the system. It is straightforward to verify that in the continuum limit the following expression reduces to (2.1.6)

$$\mathcal{H}_L = \frac{2}{a_s^2 a_t^2 g^2} \sum_j \left(2 - \mathrm{Tr} U_{x,j0}\right) + \frac{2}{a_s^4 g^2} \sum_{j<k} \left(2 - \mathrm{Tr} U_{x,jk}\right). \tag{3.1.13}$$

This allows us also to monitor the distribution of energy between electric and magnetic fields. In equation (2.1.6) the first term is the electric contribution, and the second term is the magnetic contribution.

Lattice momentum

In section 3.2 we will discuss gauge fixing on the lattice, which will be done in momentum space. Therefore we will go through the two different ways used to define momentum on the lattice. When we perform a Fourier transform from the position space to momentum space, we find out that the spacing between modes on the lattice in momentum space in the i-direction is $2\pi/L_i$, where L_i is the lattice length in the i-direction. Therefore momentum on the lattice is given by the following expression

$$\boldsymbol{p} = \frac{2\pi}{a_s} \left(\frac{m_x}{n_x}, \frac{m_y}{n_y}, \frac{m_z}{n_z}\right), \tag{3.1.14}$$

where $m_i = 0, \ldots n_i - 1$ labels the lattice site in momentum space and n_i stands for the number of lattice sites in the i-direction.

On the other hand, we can study the dispersion relation on the lattice, as done for scalar field in section 4.1.2 (where we will go through this argument in more detail). It turns out that the the dispersion relation closely resembles that of a massive particle, but the quantity which replaces the momentum is

$$\tilde{\boldsymbol{p}} = \frac{2}{a_s}\left(\sin\left(\frac{p_x a_s}{2}\right), \sin\left(\frac{p_y a_s}{2}\right), \sin\left(\frac{p_z a_s}{2}\right)\right), \tag{3.1.15}$$

where p_i are components of the lattice momentum defined by the equation (3.1.14). This will be referred to as the effective lattice momentum. With this definition the free dispersion relation $\omega^2 = \tilde{\boldsymbol{p}}^2$ holds also for scalar fields on the lattice We also note that (3.1.15) approaches (3.1.14) when values of momentum approach zero. We are not concerned by the deviations which occur in the ultraviolet, as we are interested in what happens in regime of relatively low momentum, where our theory is still accurate.

3.2 Gauge fixing on the lattice

Gauge fixing in the non-abelian case on the lattice has many similarities to the abelian continuum case, and therefore one should verify that one understands the contents of section 2.2 before proceeding to the non-abelian lattice case. Once again we will follow very closely the reference [42].

In the continuum theory, we wanted to minimize the integral in the expression (2.2.3). Its counterpart on the lattice will be the functional

$$F(U, G) = \frac{1}{2N_c}\frac{1}{4V}\sum_{x,i}\mathrm{Tr}\left(U^G_{x,i} + U^{G\dagger}_{x,i}\right), \tag{3.2.1}$$

where $U^G_{x,i} = G(x)\, U_{x,i} G^\dagger(x+\mu)$ and $G(x) = \exp\left(i\beta^a(x)\, t^a\right)$. The link matrices $U_{x,i}$ are the original links, which we want to transform to Coulomb gauge. We will minimize F by using an iterative procedure.

Now let us calculate the gradient of F with respect to the parameter β:

$$\left.\frac{\delta F}{\delta \beta^a(z)}\right|_{\beta=0} = -\frac{1}{N}\frac{1}{4V}\sum_{\mu}\mathfrak{Im}\mathrm{Tr}\left(t^a G(z)\, U_{z,\mu} G(z+\mu)^\dagger - t^a G(z-\mu)\, U_{z-\mu,\mu} G(z)^\dagger\right). \tag{3.2.2}$$

From equation (3.2.2) we see that the gradient behaves as it should - if our links are already in Coulomb gauge, the gradient at $G = \mathbb{1}$ is zero, and the right hand side corresponds to the Coulomb gauge condition.

Writing equation (3.2.2) in matrix form (using the Fierz identity) gives

$$\left.\frac{\delta F}{\delta \beta\left(z\right)}\right|_{\beta=0}=\frac{1}{16iNV}\sum_{i}\left(\Delta_{-i}\left(U_{z,i}^{G\dagger}-\text{h.c.}-\text{Tr}\right)\right), \tag{3.2.3}$$

where

$$\Delta_{-i}\left(U_{x,j}\right)=U_{x-i,j}-U_{x,j}. \tag{3.2.4}$$

h.c. stands for the hermitean conjugate, and the trace is taken over the matrix and its hermitean conjugate. From this we see that the gradient at $G=\mathbb{1}$ is

$$\frac{1}{16iNV}\sum_{i}\left(\Delta_{-i}\left(U_{z,i}^{\dagger}-\text{h.c.}-\text{Tr}\right)\right). \tag{3.2.5}$$

Analogously to the continuum theory we choose the gauge transformation matrix as

$$G\left(x\right)=\exp\left(\frac{\alpha}{2}\left(\sum_{i}\left(\Delta_{-i}\left(U_{x,i}-\text{h.c.}-\text{trace}\right)\right)\right)\right), \tag{3.2.6}$$

where α is the step length, which we want to choose as big as possible while keeping the algorithm stable. The division by two is just a convention. Now we are ready to perform the gauge transformation to the link matrices, after which we can repeat the previous step.

There is also another way to understand this algorithm. We start the algorithm with initial condition $G=\mathbb{1}$ and calculate the gradient and the first gauge transformation $G^{1}\left(x\right)$. Then we calculate $G^{2}\left(x\right)$ as the gradient of F at $G^{1}\left(x\right)$ and so on and so forth. We see that this algorithm is a steepest descent algorithm. We always take steps of a fixed length into the direction of the negative gradient, where the functional decreases the fastest.

The choice in the equation (3.2.6) corresponds to choosing $\chi=\alpha\boldsymbol{\nabla}\cdot\boldsymbol{A}$ in section 2.2. However, as before, this algorithm will suffer from critical slowing down just as the one presented in the continuum case. Once again we want to apply Fourier acceleration to this algorithm. This can be done easily, using exactly the same procedure in momentum space. The gauge transformation matrix becomes

$$G\left(x\right)=\exp\left(\hat{F}^{-1}\frac{\alpha}{2}\frac{\tilde{p}_{\text{max}}^{2}a_{s}^{2}}{\tilde{p}^{2}a_{s}^{2}}\hat{F}\left(\sum_{i}\Delta_{-i}\left(U_{x,i}-\text{h.c.}-\text{trace}\right)\right)\right), \tag{3.2.7}$$

where $\hat{F}$ stands for FFT, which in the lattice case is implemented using FFTW [46], and $\tilde{p}^{2}a_{s}^{2}$ is the lattice momentum squared multiplied by spatial lattice

spacing squared in order to make it dimensionless. It is given by the square of the effective lattice momentum (3.1.15)

$$\tilde{\boldsymbol{p}}^2 a_s^2 = 4 \sum_i \sin^2 \left(\frac{p_i a_s}{2} \right). \tag{3.2.8}$$

In (3.2.7) the parameter α has an optimal value, at least in abelian theory where the choice $\alpha = 1/k^2_{\max}$ led to convergence with just one step. In non-abelian theory this is more complicated, as we are dealing with eigenvalues of $\boldsymbol{\partial} \cdot \boldsymbol{D}$ instead of $\boldsymbol{\partial}^2$. On the lattice this gets even more complicated, and thus we choose α by trying different values and seeing which gives the best convergence. We found that values $\alpha = 0.07 - 0.08$ give the fastest convergence on our 256^2 lattice .

However the convergence of the gauge functional (3.2.1) to its minimum is rather hard to monitor, as we do not know the minimum value a priori. Therefore it is easier to monitor the divergence of the gluon field instead. The divergence on the lattice is given by

$$\Delta = \sum_i \left(U_{x-i,i} - U_{x,i} - \text{h.c.} - \text{trace} \right), \tag{3.2.9}$$

where h.c. stands for hermitean conjugate, and with trace we mean $\frac{\mathbb{1}}{N_c}\text{Tr}$ with the trace taken over everything what is to the left of it. Physically Δ is the divergence of the gluon field up to a constant. This can be seen as the expression $U_{x,i} - \text{h.c.} - \text{trace}$ gives the lattice gluon field in the matrix form (this can be seen from the equation (3.1.6). As it is easier to monitor the convergence of the divergence squared to zero as the divergence itself (as it can be negative), we define

$$\theta(x) = \text{Tr} \left(\Delta(x) \Delta^\dagger(x) \right). \tag{3.2.10}$$

And then we define

$$\theta = \frac{1}{V N_c} \sum_x \theta(x), \tag{3.2.11}$$

which will be the quantity whose convergence we monitor in our program.

4 Initial conditions and observables

4.1 Gauge fixed observables

4.1.1 Occupation number and gluon distribution function

Before we start discussing the initial conditions, we will go trough the relevant concepts in the abelian theory in order to understand their counterparts in the non-abelian theory. We should also keep in mind that most of these results cannot be derived from first principles in the non-abelian theory (where for example the particle number is not strictly speaking a well defined concept), but when the field amplitudes are sufficiently small they turn out to be fairly accurate and useful.

The gluon occupation number is given by the expression

$$\frac{\mathrm{d}N}{\mathrm{d}^3\boldsymbol{k}\mathrm{d}^3\boldsymbol{x}} = n\left(\boldsymbol{k},\boldsymbol{x}\right), \tag{4.1.1}$$

and the gluon distribution function is given by

$$\frac{\mathrm{d}N}{\mathrm{d}^3\boldsymbol{k}} = f\left(\boldsymbol{k}\right). \tag{4.1.2}$$

So the total number of particles is given by

$$N = \int \mathrm{d}^3\boldsymbol{k} f\left(\boldsymbol{k}\right), \tag{4.1.3}$$

and there is a relation between the gluon distribution function and occupation number

$$f\left(\boldsymbol{k}\right) = \int \mathrm{d}^3\boldsymbol{x} n\left(\boldsymbol{k},\boldsymbol{x}\right). \tag{4.1.4}$$

If a gluon with momentum $\boldsymbol{k}$ has energy of $\omega(\boldsymbol{k})$, the total energy of the system is

$$E = \int \mathrm{d}^3\boldsymbol{k} f(\boldsymbol{k}) \omega(\boldsymbol{k}). \tag{4.1.5}$$

We will discuss the energy of a gluon with momentum k in more detail in section 4.1.2. By using this, and the expression (2.1.6) we can establish a relation between the gluon distribution function (and occupation number) and the fields in abelian theory.

First consider the total energy of our system, which is given by

$$E = \frac{1}{2} \int \mathrm{d}^3\boldsymbol{x} \left(\boldsymbol{E}^2 + \boldsymbol{B}^2 \right). \tag{4.1.6}$$

In k-space in the Coulomb gauge (which eliminates $\boldsymbol{k} \cdot \boldsymbol{A}$) we can write this as

$$E = \frac{1}{2} \frac{1}{(2\pi)^3} \int \mathrm{d}^3\boldsymbol{k} \left(|\boldsymbol{E}(\boldsymbol{k})|^2 + \boldsymbol{k}^2 |\boldsymbol{A}_C(\boldsymbol{k})|^2 \right), \tag{4.1.7}$$

where the subscript C stands for Coulomb gauge. This intermediate step is also covered in detail in the appendix A.2. There we will go through the use of Parseval theorem, which we will use repeatedly in this section.

Now inspect energy of a single mode lying between k and $k + \mathrm{d}k$, equating the expressions above and assuming $\omega(\boldsymbol{k}) = |\boldsymbol{k}|$ we get

$$f(\boldsymbol{k}) = \frac{1}{2} \frac{1}{(2\pi)^3} \left(\frac{|\boldsymbol{E}(\boldsymbol{k})|^2}{|\boldsymbol{k}|} + |\boldsymbol{k}| |\boldsymbol{A}_C(\boldsymbol{k})|^2 \right). \tag{4.1.8}$$

Assuming roughly equal distribution of energy between electric and magnetic modes, i.e. $\left|\boldsymbol{E}^2\right| = \left|\boldsymbol{B}^2\right| = \boldsymbol{k}^2 |\boldsymbol{A}_C|^2$ one can also derive other equivalent expressions for the particle distribution

$$f(\boldsymbol{k}) = \frac{1}{(2\pi)^3} |\boldsymbol{k}| |\boldsymbol{A}_C(\boldsymbol{k})|^2 = \frac{1}{(2\pi)^3} \frac{|\boldsymbol{E}(\boldsymbol{k})|^2}{|\boldsymbol{k}|} = \frac{1}{(2\pi)^3} \sqrt{|\boldsymbol{E}(\boldsymbol{k})|^2 |\boldsymbol{A}_C(\boldsymbol{k})|^2}. \tag{4.1.9}$$

All of the expressions above are equivalent in the time averaged abelian theory. The difference between the occupation number and the gluon distribution function is a factor of V, which appears from integration of the equation (4.1.4).

When we refer to the occupation number distribution in this work, we will use the following expressions

$$n_{AE}(t, \boldsymbol{k}) = \frac{1}{(2\pi)^3 V} \sqrt{\langle |\boldsymbol{E}(t, \boldsymbol{k})|^2 \rangle \langle |\boldsymbol{A}_C(t, \boldsymbol{k})|^2 \rangle}. \tag{4.1.10}$$

$$n_A(t,\boldsymbol{k}) = \frac{1}{(2\pi)^3 V}|\boldsymbol{k}||\boldsymbol{A}_C(t,\boldsymbol{k})|^2 \tag{4.1.11}$$

$$n_E(t,\boldsymbol{k}) = \frac{1}{(2\pi)^3 V}\frac{|\boldsymbol{E}(t,\boldsymbol{k})|^2}{|\boldsymbol{k}|}. \tag{4.1.12}$$

4.1.2 Dispersion relation

Dispersion relation in QED

In chapter 3 we saw how we can solve the time evolution of the gauge fields and the electric fields on the lattice. Now we would like to establish a link between the particle interpretation of our theory (which we had above) and the field interpretation which will be used in the calculations. We will start looking for this connection from the equations of motion of QED

$$\partial_\mu F^{\mu\nu} = 0 = \partial^2 A^\nu - \partial^\nu \partial \cdot A = 0. \tag{4.1.13}$$

In Coulomb gauge, using the definition of the electric field, we get

$$-\boldsymbol{\nabla}^2 A_C^\nu - \partial_t E^\nu = 0. \tag{4.1.14}$$

Taking the Fourier transform this becomes

$$\boldsymbol{k}^2 A_C^\nu(k) + i\omega E^\nu(k) = 0. \tag{4.1.15}$$

Then we solve for ω, take the absolute value squared of both sides and sum over Lorentz indices. We get

$$\omega^2(k) = \boldsymbol{k}^4 \frac{|\boldsymbol{A}_C(k)|^2}{|\boldsymbol{E}(k)|^2}. \tag{4.1.16}$$

Using equation (4.1.16), the fact that in Coulomb gauge $|\boldsymbol{B}_C| = \boldsymbol{k}^2 |\boldsymbol{A}_C(\boldsymbol{k})|^2$ and assuming equal distribution of energy between electric and magnetic field modes we find the free dispersion relation $\omega^2(\boldsymbol{k}) = \boldsymbol{k}^2$. Using this we get

$$\omega^2(k) = \frac{|\boldsymbol{E}(k)|^2}{|\boldsymbol{A}_C(k)|^2}. \tag{4.1.17}$$

For the non-abelian theory we take (4.1.17) as the definition of $\omega^2(k)$ and use it to study modifications to the free dispersion relation $\omega(k) = |\boldsymbol{k}|$ arising

from the interactions - in particular mass. The thermal field theory predicts that gluons can obtain effective mass due to the interactions, and the equation (4.1.17) allows us to see if the Yang-Mills theory predicts similar behaviour. If we use this along with (4.1.9), we can also calculate the total energy of the system using (4.1.5). Comparing the result with the one we get using (3.1.13) we can check how close the results given by these two alternative approaches are from one another. If these two are in agreement, we can safely interpret our results using the expressions which are derived in the abelian theory. We can also calculate a prediction for the total energy using the abelian theory (which assumes $\omega \approx |\boldsymbol{k}|$) when we specify the gluon distribution function. We expect that this should be in good agreement with the results obtained using (3.1.13) and (4.1.5) when the field amplitudes are small. As the field amplitudes grow bigger we expect bigger deviation due to the gluon Debye mass.

Dispersion relation on the lattice

Before we go deeper into the gluon dispersion relation in the lattice gauge theory, we will go through an illustrating example in the scalar field theory. Consider a massive scalar field given by the Lagrangian density

$$\mathcal{L} = \frac{1}{2}\left(\partial_\mu \phi\right)^2 - \frac{1}{2}m^2\phi^2. \tag{4.1.18}$$

The equation of motion is

$$\left(\Box + m^2\right)\phi\left(x\right) = 0. \tag{4.1.19}$$

We can solve this using an ansatz

$$\phi\left(x\right) = A\exp\left(ip\cdot x\right). \tag{4.1.20}$$

By direct substitution we find

$$\omega^2 = \boldsymbol{p}^2 + m^2, \tag{4.1.21}$$

which is exactly what we wanted to find. However, in discretised theory the dispersion relation is not the same as in continuum theory. Now let us perform spatial discretisation while keeping time as a continuous variable. For simplicity we discretise the space into a cubic lattice (a similar argument would carry over to any rectangular lattice) of N^3 points with lattice spacing a_s. As a result our spatial coordinates are restricted to the set $x = \left(m_x a_s, m_y a_s, m_z a_s\right)$, where $m_i = 0, \ldots N-1$. By imposing periodic boundary conditions the allowed

wavevectors are $k = \frac{2\pi}{Na_s}\left(m_x, m_y, m_z\right)$. We discretise the derivatives as (no summation over i here)

$$\partial_i^2\phi\left(x\right) = \frac{\phi\left(x + a_s\hat{i}\right) + \phi\left(x - a - s\hat{i}\right) - 2\phi\left(x\right)}{a_s^2}. \tag{4.1.22}$$

The discretised equation of motion becomes

$$\partial_t^2\phi\left(x\right) - \nabla_L^2\phi\left(x\right) + m^2\phi\left(x\right) = 0, \tag{4.1.23}$$

where ∇_L^2 is the lattice laplacian discretised as in equation (4.1.22). By plugging in the ansatz (4.1.20) and simplifying we get

$$\omega^2 - \frac{4}{a_s^2}\left(\sin^2\left(\frac{k_x a_s}{2}\right) + \sin^2\left(\frac{k_y a_s}{2}\right) + \sin^2\left(\frac{k_z a_s}{2}\right)\right) - m^2 = 0. \tag{4.1.24}$$

This equation closely resembles the dispersion relation of a relativistic massive particle

$$\omega^2\left(\boldsymbol{p}\right) = \boldsymbol{p}^2 + m^2. \tag{4.1.25}$$

Comparing the equations (4.1.24) and (4.1.25) we see that it makes sense to define the effective lattice momentum, which we already defined in (3.1.15), as

$$\tilde{\boldsymbol{p}}^2 = \frac{4}{a_s^2}\left(\sin^2\left(\frac{p_x a_s}{2}\right) + \sin^2\left(\frac{p_y a_s}{2}\right) + \sin^2\left(\frac{p_z a_s}{2}\right)\right), \tag{4.1.26}$$

where $p_i = \frac{2\pi}{Na_s} m_i$, $m_i = 0 \ldots N-1$.

From the equation (4.1.24) we see that the lattice dispersion relation is indeed different from the continuum dispersion relation (it has the same continuum limit though). And there is also a fundamental difference in the way it treats different momentum modes with same magnitude: ω may be different for two modes, for which $|\boldsymbol{p}_1| = |\boldsymbol{p}_2|$, which does not happen in the continuum. One should also note that the dispersion relation on the lattice depends on the chosen discretisation scheme. For dispersion relations in different discretisation schemes (for scalar fields) see for instance [47].

The dispersion relation is actually gauge dependent. In QED in Coulomb gauge one can show (as done in section 4.1.2) that the dispersion relation is given by the expression

$$\omega^2\left(\boldsymbol{k}\right) = \frac{\langle|\boldsymbol{E}\left(\boldsymbol{k}\right)|^2\rangle}{\langle|\boldsymbol{A}_C\left(\boldsymbol{k}\right)|^2\rangle}. \tag{4.1.27}$$

Debye mass

The plasmon mass, which in this case is equal to the Debye mass, can be obtained using this relation when $\boldsymbol{k} \to 0$ as

$$m_{pl} = \omega\left(\boldsymbol{k} = 0\right). \tag{4.1.28}$$

We should keep in mind that different modes have different relaxation times, and for the zero mode the relaxation time turns out to be infinite. Therefore we have to extrapolate the value of the plasmon mass from our results.

The plasmon mass can also be calculated from thermal field theory. This will serve as an important cross-check for our result. The expression for the Debye mass is [38]

$$m_D^2 = 4g^2 N_c \int \frac{\mathrm{d}^3\boldsymbol{k}}{(2\pi)^3} \frac{n\left(\boldsymbol{k}\right)}{|\boldsymbol{k}|}. \tag{4.1.29}$$

We can evaluate this expression on the lattice by discretising the integral with the substitution $\int \mathrm{d}^3\boldsymbol{k} \to \sum_{\boldsymbol{k}} \frac{(2\pi)^3}{V}$. We get

$$m_D^2 = 4g^2 N_c \sum_{\boldsymbol{k}} \frac{n\left(\boldsymbol{k}\right)}{|\boldsymbol{k}|V}. \tag{4.1.30}$$

Equation (4.1.29) also gives us an important link between the occupation numbers and gluon Debye mass. The Debye mass is a time dependent quantity, but its time dependence is governed by the time-evolution of the occupation number distribution.

Coulomb gauge occupation number

In the Coulomb gauge we can make an order of magnitude estimate for the occupation number as follows. We get the total number of particles by using equation (4.1.3) along with equation (4.1.9). The estimate is finally obtained by dividing the particle number by the volume and size of the phase space, which is roughly Δ^2 in our case. Thus we define (in two dimensions)

$$n_0^N = \frac{N}{L^2} \frac{(2\pi)^2}{\Delta^2}. \tag{4.1.31}$$

Physically this parameter tells us the average occupation number of our system. If $n_0^N \gg 1$ we are in the regime in which the classical statistical approximation is valid, and thus our results are applicable to physically relevant scenarios.

4.2 Gauge invariant observables

4.2.1 Typical momentum squared

We want to study particle number distributions with typical momentum scale Δ, which will later appear in our initial condition. However, as the gluon fields are not gauge invariant, this is not a unique way to define our typical momentum scale in the problem. One convenient way to define the typical momentum scale gauge invariantly on the lattice is [38]:

$$\langle \boldsymbol{k}^2 \rangle_{KM} = \frac{\int \mathrm{Tr}\left(\boldsymbol{D} \times \boldsymbol{B}\right)^2 \mathrm{d}^3 x}{\frac{1}{2}\int \mathrm{Tr}\left(\boldsymbol{E}^2 + \boldsymbol{B}^2\right) \mathrm{d}^3 x}. \tag{4.2.1}$$

The equation (4.2.1) can be justified from classical electrodynamics. Consider the expression

$$\langle \boldsymbol{k}^2 \rangle = \frac{\int \left(\boldsymbol{\nabla} \times \boldsymbol{B}\right)^2 \mathrm{d}^3 x}{\frac{1}{2}\int \left(\boldsymbol{B}^2 + \boldsymbol{E}^2\right) \mathrm{d}^3 x}, \tag{4.2.2}$$

which corresponds to equation (4.2.1) in the classical electrodynamics. Decomposing $\boldsymbol{B}$ and $\boldsymbol{E}$ in Fourier-modes and assuming no angular dependence we get

$$\langle \boldsymbol{k}^2 \rangle = \frac{\int k^4 |\boldsymbol{B}(k)|^2 \mathrm{d}k}{\frac{1}{2}\int k^2 \left(|\boldsymbol{B}(k)|^2 + |\boldsymbol{E}(k)|^2\right) \mathrm{d}k}. \tag{4.2.3}$$

Now parametrically $|\boldsymbol{B}(k)|^2 \sim |\boldsymbol{E}(k)|^2 \sim k f(k)$, so this can be seen as a parametric order of magnitude estimate for the expectation value of momentum squared

$$\langle \boldsymbol{k}^2 \rangle \approx \frac{\langle k^5 \rangle}{\langle k^3 \rangle}. \tag{4.2.4}$$

We will also use a slightly modified version of the equation (4.2.1) [48].

$$\langle \boldsymbol{p}^2 \rangle_{BR} = \frac{\int \mathrm{Tr}\left(\boldsymbol{D} \times \boldsymbol{B}\right)^2 \mathrm{d}^3 x}{\int \mathrm{Tr}\left(\boldsymbol{B}^2\right) \mathrm{d}^3 x}. \tag{4.2.5}$$

Equation (4.2.5) is equivalent to (4.2.1) when the electric and magnetic energies are approximately equal. Using equation (4.2.5) equation (4.2.3) becomes

$$\langle \boldsymbol{p}^2 \rangle = \frac{\int k^4 |\boldsymbol{B}(k)|^2 \mathrm{d}k}{\int k^2 |\boldsymbol{B}(k)|^2 \mathrm{d}k}. \tag{4.2.6}$$

Equation (4.2.5) is better suited for calculating average value for momentum squared from our initial conditions, which contain purely magnetic energy. Equations (4.2.1) and (4.2.5) are equal, when the total energy of the system is equally divided between the electric and magnetic fields. The system also tends to evolve into a state, in which the electric and magnetic energies are approximately equal due to the equipartition of energy in the classical theory. However, as our initial conditions contain purely magnetic energy, the numerator in equation (4.2.1) is two times larger at $t = 0$ than at the time when the energy of the system is equally distributed between electric and magnetic fields. This means that we need to adjust normalization in equation (4.2.1). Thus we take (4.2.5) as the definition of momentum squared at $t = 0$.

The lattice implementation of these gauge invariant momentum estimates is discussed in detail in appendix D.

4.2.2 Occupation number

We would like to find a sufficient order of magnitude estimate for the occupation number of our system. We can estimate the particle number by dividing the total energy of our system by the typical momentum of a single particle. From this we get the occupation number by dividing by the volume in position space, and by the size of the phase space, which in our case will be roughly Δ^2 in two dimensions. Thus we define

$$n_0^E = \frac{E}{L^2\sqrt{\langle k^2 \rangle}_{KM}} \frac{(2\pi)^2}{\Delta^2} \tag{4.2.7}$$

This quantity has a similar interpretation as n_0^N defined in (4.1.31), and their values should be in rough agreement. Thus they can be used as a cross-check. Later we will study both of these quantities numerically and analytically.

4.3 Initial conditions

For initial conditions we choose a scenario similar to [32]. We set the electric fields to zero (this is by far the easiest way to satisfy the Gauss constraint). We

sample the gauge fields from the following distribution

$$\langle A_i^a(p) A_j^{\dagger b}(q)\rangle = \frac{2}{3}\frac{2\pi}{\left(N_c^2-1\right)(D-1)}\delta_{ij}\delta^{ab}\frac{(2\pi)^3\delta(p-q)}{V}\frac{C}{(2\pi)^{3/2}\Delta^2\Delta_z} \exp\left(-\frac{p_t^2}{2\Delta^2}-\frac{p_z^2}{2\Delta_z^2}\right) \tag{4.3.1}$$

Here Δ is the transverse momentum scale, which can be associated to the saturation scale Q_s [49], and Δ_z is the longitudinal momentum scale. Typically we choose s.t. $\Delta \gg \Delta_z$, and set Δ_z to such a small value, that the longitudinal distribution essentially resembles a delta function distribution. By N_c we denote the number of colors and D is the number of space-time dimensions. In our code D will always be equal to four, and in analytical calculations D will be equal to four when we calculate estimates in three spatial dimensions, and three, when we are considering estimates in two spatial dimensions. Instead of D, we have a factor of $D-1$ in the denominator in (4.3.1). This is because we are working in temporal gauge, in which the temporal component of the gluon field does not contribute.

The dimensionful parameters appearing in equation (4.3.1) are C and Δ. Obviously $[\Delta] = \text{GeV}$ as it represents the momentum scale. We deduce the dimensions of C by starting from the fact that action has to be dimensionless, thus $\int A^4(x)\,\mathrm{d}^4x$ is dimensionless. Thus $[A(x)] = \text{GeV}$. In momentum space $[A(p)] = \text{GeV}^{-2}$ as it is obtained by integrating over three spatial dimensions when Fourier transformed. Therefore $A^2(p)$ has dimensions of $1/\text{GeV}^4$. In order to achieve this C must have dimensions of $1/\text{GeV}$.

In two dimensions equation (4.3.1) becomes

$$\langle A_i^a(p) A_j^{\dagger b}(q)\rangle = \frac{2}{3}\frac{L_z}{\left(N_c^2-1\right)(D-1)}\delta_{ij}\delta^{ab}\frac{(2\pi)^3\delta(p-q)}{V}\frac{C}{2\pi\Delta^2} \exp\left(\frac{-p_t^2}{2\Delta^2}\right)\frac{\delta(p_z)(2\pi)}{L_z},$$

where L_z is the length of our system in the z-direction. Thus the expectation value of the field squared in three dimensions is

$$\langle |\boldsymbol{A}(\boldsymbol{p}, t=0)|^2\rangle = \frac{2C}{3(2\pi)^{1/2}\Delta^2\Delta_z}\exp\left(-\frac{\boldsymbol{p_t}^2}{2\Delta^2}-\frac{p_z^2}{2\Delta_z^2}\right) \approx \frac{1}{(2\pi)^3}\frac{f(\boldsymbol{p})}{|\boldsymbol{p}|}. \tag{4.3.2}$$

As we are interested in studying a two-dimensional system, we take the limit $\Delta_z \to 0$, and using the identity $\frac{1}{a\sqrt{\pi}} \exp\left(-x^2/a^2\right) \xrightarrow[a\to 0]{} \delta(x)$ equation (4.3.2) becomes

$$\langle |\boldsymbol{A}(\boldsymbol{p}, t=0)|^2 \rangle = \frac{L_z}{(2\pi)} \frac{2}{3} \frac{C}{\Delta^2} \exp\left(-\frac{\boldsymbol{p_t}^2}{2\Delta^2}\right) \frac{(2\pi)\,\delta(\boldsymbol{p_z})}{L_z}. \tag{4.3.3}$$

As some of our observables are meaningful only in the Coulomb gauge, we will next calculate the expectation value of the gluon field squared in that gauge. In the Coulomb gauge the projection of the gluon field on the momentum vector is always zero. Thus, we get the gluon field (using an abelian approximation) in the Coulomb gauge as

$$A^a_{C,i}(p) = \left(\delta_{ij} - \frac{p_i p_j}{p^2}\right) A^a_j(p). \tag{4.3.4}$$

This corresponds to choosing $\chi = {}^{p_j A_j}/_{p^2}$ analogously to equation (2.2.12). In non-abelian case there is no easy way to do similar procedure analytically. Using this the expectation value of the gluon field squared in the Coulomb gauge becomes

$$\langle \left| A^a_{C,i}(p) \right| \rangle = \langle A^a_i(p)\, A^{\dagger a}_i(p) \rangle - \frac{p_i p_h}{p^2} \langle A^a_i(p)\, A^{\dagger a}_h(p) \rangle. \tag{4.3.5}$$

Using the initial condition (4.3.1) and simplifying we get

$$\langle |A_C(p)|^2 \rangle = \frac{D-2}{D-1} \langle |A(p)|^2 \rangle, \tag{4.3.6}$$

Thus the expected value of the gluon field squared in the Coulomb gauge is two thirds of that we get using the initial condition.

Meaningful lattice quantities

In lattice field theory no dimensionful quantity is meaningful per se, for example the numerical value of momentum scale does not tell us anything, unless we compare it to some other quantity.

Next we will derive a quantity which gives us an estimate how large the occupation numbers we have actually are. We start from Fermi-Dirac statistics. For massless fermions the distribution for energy (or momentum) for single particle states is

$$n(k_i) = \frac{1}{\exp\left(\frac{k_i - \mu}{T}\right) + 1}. \tag{4.3.7}$$

If we approximate this with continuous distribution at zero temperature the distribution becomes a step function distribution, and thus the total particle number is

$$N = \int \frac{\mathrm{d}^d k \mathrm{d}^d x}{(2\pi)^d} \theta (k - \mu) . \tag{4.3.8}$$

From this expression we can identify the occupation number distribution as $n(k) = 1/(2\pi)^3 \theta(k-\mu)$. Thus for fermions there is a single fermion in each state in our system when $n(k) = 1/(2\pi)^3$. We can use this fact to approximate the occupation number in our (bosonic) system.

We start from expression (4.1.11) in four space-time dimensions. Plugging in the gluon field squared in the Coulomb gauge yields the expression

$$n_A(k) = \frac{1}{(2\pi)^3} \frac{4}{9} \frac{C\Delta}{3\sqrt{2\pi}\Delta^2 \Delta_z V} \frac{|k|}{\Delta} \exp\left(-\frac{k_t^2}{2\Delta^2} - \frac{k_z^2}{2\Delta_z^2} \right). \tag{4.3.9}$$

Comparing this with (4.3.8) inspires us to define

$$n_0^{3d} = \frac{4}{9} \frac{C\Delta}{\sqrt{2\pi}\Delta^2 \Delta_z V}. \tag{4.3.10}$$

This parameter tells us how large the occupation number for the mode with highest occupancy is , as for the highest occupancy mode $|k|/\Delta \exp\left(-k_t^2/2\Delta^2 - k_z^2/2\Delta_z^2\right) \sim 1$. We also see that n_0^{3d} is dimensionless and independent of the volume of our system. We can define the corresponding quantity in two dimensional case by taking the limit $\Delta_z \to 0$ in expression (4.3.9). We get

$$n_A(k) = \frac{1}{(2\pi)^4} \frac{4}{9} \frac{C\Delta}{3\Delta^2 V_{2d}} \frac{|k|}{\Delta} \exp\left(-\frac{k_t^2}{2\Delta^2} \right) \frac{(2\pi)\delta(k_z)}{L_z}, \tag{4.3.11}$$

where V_{2d} is the two dimensional volume defined as $V_{2d} = L_x L_y$. Using this we define the two dimensional counterpart of n_0^{3d} as

$$n_0^{2d} = \frac{1}{(2\pi)^2} \frac{4}{9} \frac{C}{V_{2d}\Delta}. \tag{4.3.12}$$

Now we can write (4.3.11) using n_0^{2d}

$$n_A(k) = \frac{n_0^{2d}}{12\pi^2} \frac{|k|}{\Delta} \exp\left(-\frac{k_t^2}{2\Delta^2} \right) \frac{(2\pi)\delta(k_z)}{L_z} \tag{4.3.13}$$

4.3.1 Related observables

We will now approximate analytically the relevant observables presented in sections 4.1 and 4.2 at $t = 0$. This forces us to take (4.1.11) as the definition of occupation number distribution, as our initial conditions contain purely magnetic energy. This will also change the normalisation of n_A in this section. Because the equivalence of the different definitions of the occupation number is based on the approximation that the energy stored in electric and magnetic fields is approximately equal, we will have to divide the initial occupation number distribution (4.3.13) by two while performing these calculations. This difference in normalisation is analogous to the difference between the definitions of $\langle k^2 \rangle_{KM}$ and $\langle p^2 \rangle_{BR}$, appearing in equations (4.2.1) and (4.2.5). There (4.2.5) is more suitable for our initial condition and turns out to yield consistent results with (4.2.1) at later times. We will present some predictions for the three dimensional case, but mostly we will focus on the two dimensional case, which we will later study numerically.

We get the total particle number of our system by integrating equation (4.1.1). Plugging in the distribution function in Coulomb gauge and doing the relevant integrals in cylindrical coordinates gives

$$N = \frac{C\left(\frac{\Delta^2 \cos^{-1}\left(\frac{\Delta z}{\Delta}\right)}{\sqrt{(\Delta - \Delta z)(\Delta + \Delta z)}} + \Delta z\right)}{9\sqrt{2}\pi^{5/2}}. \tag{4.3.14}$$

In the limit $\Delta_z \to 0$ we get

$$N_{\Delta_z = 0} = \frac{C\Delta}{18\sqrt{2}\pi^{3/2}}. \tag{4.3.15}$$

Using the two dimensional occupancy parameter n_0^{2d} this becomes

$$N_{\Delta_z = 0} = \frac{1}{2}\sqrt{\frac{\pi}{2}}\Delta^2 n_0^{2d} V_{2d}. \tag{4.3.16}$$

Similarly we can calculate the total energy of the system in these cases. The total energy is given by the equation (4.1.6). We approximate the dispersion relation with the free massless dispersion relation $\omega = |k|$. Once again we do the integrals in cylidrical coordinates. We get

$$E = \frac{C\left(2\Delta^2 + \Delta_z^2\right)}{18\pi^2}. \tag{4.3.17}$$

The two dimensional formula for the total energy in the limit $\Delta_z \to 0$ using the two dimensional occupancy parameter is

$$E_{\Delta_z=0} = \Delta^3 n_0^{2d} V_{2d}. \tag{4.3.18}$$

We can also calculate the average momentum squared as in (4.2.6). We make use of the fact that in the Coulomb gauge $|\boldsymbol{B}|^2 = |\boldsymbol{k}|^2 |\boldsymbol{A}|^2$. We get

$$\langle k^2 \rangle_{BR} = -2\Delta^2 + \frac{12\Delta^4}{2\Delta^2 + \Delta_z^2} + 3\Delta_z^2. \tag{4.3.19}$$

Thus the prediction for the averaged momentum squared using the gauge invariant estimator is $\langle \boldsymbol{k}^2 \rangle_{BR} = 4\Delta^2$.

If we plug in the initial occupation number distribution (4.3.11) we can easily calculate the integral in the equation (4.1.29). The initial value of the gluon Debye mass is

$$m_D^2 = \frac{C g^2 N_c}{36\pi^5 V}. \tag{4.3.20}$$

Writing this in two dimensions using the two dimensional occupancy parameter gives

$$m_D^2 = \frac{g^2 n_0^{2d} N_c \Delta}{4\pi^3 L_z}. \tag{4.3.21}$$

Due to the time evolution of the gluon distribution function this value is not constant in time, but it still serves as an order of magnitude estimate for the Debye mass. At first sight the $1/L_z$ dependence of the Debye mass appearing in equation (4.3.21) seems somewhat bizarre. This is caused by the fact that we parametrized the Debye mass with n_0^{2d}, which includes only two dimensional volume as we needed $1/L_z$ for the normalisation of $\delta(p_z)$ appearing in equation (4.3.3). In three dimensions, using n_0^{3d}, no such problems arise. Solving n_0^{2d} from equation (4.3.10) for C/V and plugging in (4.3.20) yields $m_D^2 \sim n_0^{3d} \Delta \Delta_z$. It should be noted that m_D^2 does not vanish as $\Delta_z \to 0$ as n_0^{3d} is proportional to $1/\Delta_z$. Thus m_D^2 behaves as it should with three dimensional parametrisation. Finally one should note, that in two dimensions we run our code with $256 \times 256 \times 1$ lattice. Thus L_z is regularised with lattice spacing in numerical calculations such that $L_z = a_s$.

We expect that the results derived in this section hold when we are "close" to the abelian theory, i.e. when the field amplitudes are small. This is mainly controlled by the parameter C in (4.3.2), or equivalently the more physically meaningful parameter n_0^{2d}. We can also verify this from equation (4.3.14) or

(4.3.16). However, as we increase the numerical value of n_0^{2d} we depart further from the "abelian regime" of our theory, and our results will start to differ from the ones we obtained by analytical approximations in this section. Even in this regime the abelian results will still serve as important order of magnitude estimates.

4.3.2 Practical implementation

In practice we implement the initial condition (4.3.2) as follows. We get the gauge fields in the position space by doing the inverse Fourier transform on the field in momentum space

$$\boldsymbol{A}\left(\boldsymbol{x}, t=0\right)=\frac{1}{\left(2\pi\right)^3}\int \mathrm{d}^3\boldsymbol{p}\boldsymbol{A}\left(\boldsymbol{p}, t=0\right)\exp\left(i\boldsymbol{p}\cdot\boldsymbol{x}\right), \tag{4.3.22}$$

where $\boldsymbol{A}\left(\boldsymbol{p}, t=0\right)$ is given by (4.3.2). This is then discretised by turning the integral into a sum over all possible momenta $\int_{\boldsymbol{p}} \mathrm{d}^3\boldsymbol{p} \to \sum_{\boldsymbol{p}} a_p^3$, where a_p is the lattice spacing in momentum space. In momentum space the spacing between different momentum modes is $\frac{(2\pi)}{L}$, where L is the lattice length in the given direction. Thus $a_p^3=\frac{(2\pi)^3}{V}$, where V is the lattice volume. Now we substitute the expression (4.3.2) into (4.3.22) and replace the sum over momentum modes by sum over lattice sites. We get

$$\boldsymbol{A}_k=\frac{1}{V}\sum_{\boldsymbol{m}}\boldsymbol{A}_{\boldsymbol{m}}\exp\left(2\pi i\frac{\boldsymbol{m}}{\boldsymbol{n}}\cdot\boldsymbol{k}\right), \tag{4.3.23}$$

where we have also made substitution $x=a_s\left(k_x,k_y,k_z\right)$, and adopted the multi-index notation for the momentum modes $\frac{\boldsymbol{m}}{\boldsymbol{n}}=\left(\frac{m_x}{n_x},\frac{m_y}{n_y},\frac{m_z}{n_z}\right)$. This is simply the discrete inverse Fourier transform of $\boldsymbol{A}\left(\boldsymbol{p}\right)$ normalized with lattice volume. Fourier transforms are covered in more detail in the appendix A.

We use the FFTW library [46] to perform the Fourier transforms. When we have calculated the gluon fields in position space, it is straightforward to calculate the links using the definition of the link matrix (3.1.1).

As we are interested in two dimensional situation, we set the lattice length in the longitudinal direction to 1 instead of performing dimensional reduction to the theory. In practise this means that we have only zero momentum modes available in the longitudinal direction. As a consequence these modes are global in position space, so there will be no z-dependence there either.

We implement the gluon distribution as follows. First we set all fields with same momenta to a constant value in color and direction, and we assign the same value in the real and imaginary part. This constant value is chosen such that summing over colors and directions we recover the expectation value appearing in (4.3.3). Then each component of the field (i.e. color, direction and real and imaginary part) is multiplied by a gaussian random number x. These random numbers are chosen such that $\langle x \rangle = 0$, so they are centered around zero, but $\langle x^2 \rangle = 1$.

As noted in appendix A, a Fourier transform of real data possesses hermitean symmetry. This means that roughly half of the data is redundant, some frequencies can be obtained as complex conjugates of others as explained in A. We force our complex data to obey this symmetry, by checking explicitly for each complex frequency whether if has a conjugate frequency, and if it does, we set the values of our fields accordingly. Some frequencies, like zero frequency, are real and thus they are their own complex conjugates. Real frequencies can be treated with the same procedure, as they are their own conjugate frequencies.

5 Results

5.1 Practicalities

All results presented in this chapter have been obtained using a 256^2 lattice with only one point in the longitudinal direction. For parameters we used $a_s = 1$, $g = 1$, $a_s\Delta = 0.3$ and $a_t = 0.01a_s$. The gauge fixing parameters used were $\alpha = 0.07$ and the criterion for stopping the iterative gauge fixing procedure was $\theta < 10^{-10}$. The values of $\langle|\boldsymbol{A}(\boldsymbol{k})|^2\rangle$ and $\langle|\boldsymbol{E}(\boldsymbol{k})|^2\rangle$ were recorded in Coulomb gauge at dimensionless times $t\Delta = 3, 6, 9 \ldots, 30$. In practice this was done by averaging over all angles and 10 runs (i.e. averaged over 10 initial conditions). The range of available lattice momenta squared between 0 and $\tilde{k}^2_{\text{max}}$ were divided in equally large bins in $\boldsymbol{k}^2$ and the amount of bins used in all runs was 10000. The values of $\langle|\boldsymbol{A}(\boldsymbol{k})|^2\rangle$ and $\langle|\boldsymbol{E}(\boldsymbol{k})|^2\rangle$ were then chosen to represent average $\boldsymbol{k}^2$ in their bins. From these observables we can then reconstruct the gluon distribution function using equation (4.1.9), the occupation number distribution using equation (4.1.10) and the dispersion relation using (4.1.17). These can then be used to calculate the total energy of the system, which can be compared to the one we get from plaquettes. When we calculated the total energy of the system, we used the n_{AE} definition of the occupation number (4.1.10). At these same instants of time we also calculated the expectation value of the average momentum squared using (4.2.1). This can then be compared to the value we get using the abelian approximation (4.3.19).

5.2 Dispersion relation

We start by studying the gluon dispersion relation given by equation (4.1.27). As stated in section 5.1, we fixed Coulomb gauge every thousandth timestep, and recorded the values of the modulus of the color electric fields and color magnetic fields. From these we are able to reconstruct the approximate dispersion relation for gluons using equation (4.1.27).

In figure 5.1, we have the time evolution of a typical dispersion relation in dimensionless time. We observe that at early times the dispersion relation is oscillating, but at late times we observe a linear dispersion relation at low momenta. These oscillations arise, because the solutions of the non-interacting theory are plane waves, and thus on a very schematic level the solutions are of the form $A \sim \cos(|k|\, t)$ and thus $E \sim \sin(|k|\, t)$. Therefore $\omega \sim \tan(|k|\, t)$. From this we can deduce that dispersion relation should have peaks and dips in k whose distance from one another is proportional to $1/t$. From the figure 5.1 we observe that at $t\Delta = 6$ there are roughly 1.5 oscillations between $k^2/\Delta^2 = 40$ and $k^2/\Delta^2 = 50$. For $t\Delta = 12$ the corresponding value is 3, for $t\Delta = 18$ 4.5 and for $t\Delta = 24$ we find ~ 6 oscillations. Thus we observe that the period of oscillations in k doubles as we double the amount of time elapsed. At $t\Delta = 30$. we can not observe these oscillations anymore. The reason for this is that the non-abelian effects cause the decoherence by introducing a coupling between different modes.

The equilibration speed does not depend only on time, but also on the value of the parameter n_0^{2d}. This is quite natural, as n_0^{2d} gives the amplitude of the gluon field, and therefore the non-abelian interactions are stronger at larger n_0^{2d}, which leads to shorter decoherence time.

Figure 5.2 shows a typical late time dispersion relation. As the oscillations have already decohered at these times, we can meaningfully extract the Debye screening mass by doing a linear fit in the low momentum regime. In the figure 5.2, we chose the momentum regime to be $\tilde{k}^2/\Delta^2 \leq 1/2$ (as in all other fits done in this work).

In figure 5.3, we have plotted the dispersion relations at different times. This time we used a logarithmic scale to enhance the low momentum regime. We also performed linear fits to the data in the same momentum regime as before, and we see that the value of the Debye screening mass tends to decrease as we go to higher dimensionless times. The fact that the value of the Debye mass seems to be higher for $t\Delta = 12$ than for $t\Delta = 18$ in figure 5.3 is likely caused by low statistics.

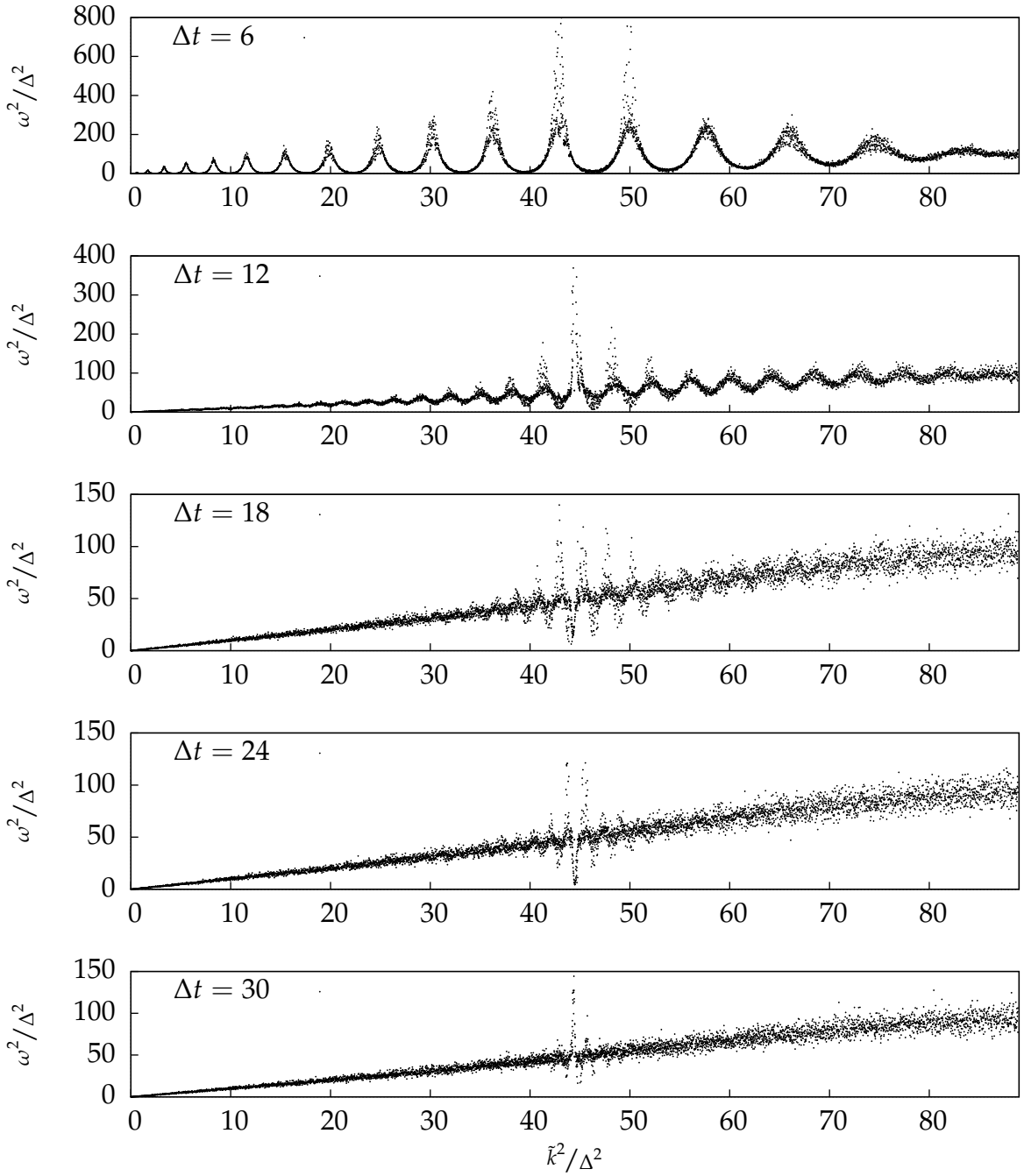

Figure 5.1: Typical time-evolution of the dispersion relation. The value of the parameter n_0^{2d} used was 0.028. The time evolution for other values of n_0^{2d} is qualitatively similar, but the speed of decoherence varies depending on the value of n_0^{2d}. Systems with higher value of n_0^{2d} decohere faster than the ones with a lower value.

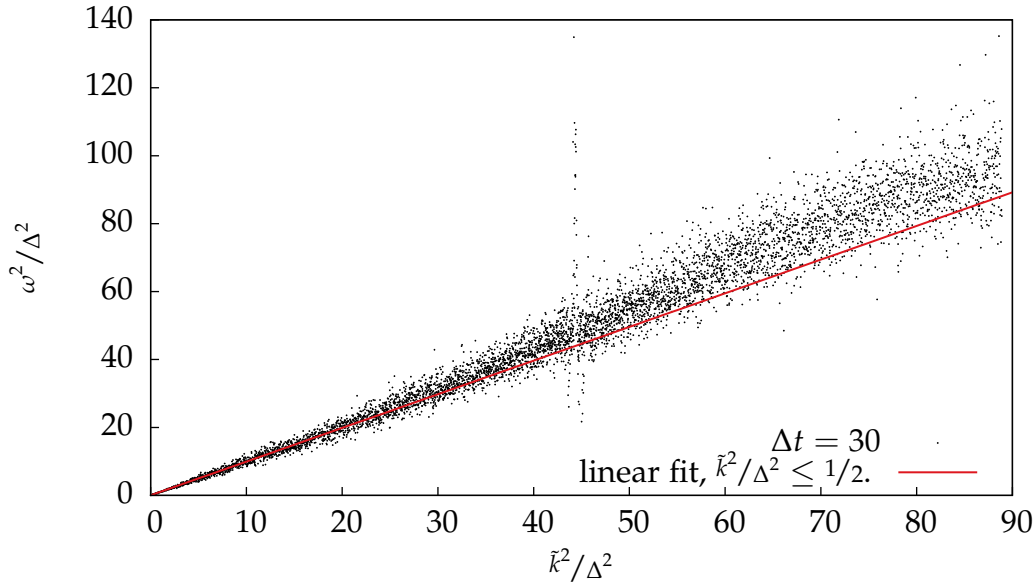

Figure 5.2: Typical dispersion relation at late times. The value obtained for the Debye mass from the fit was $m_D^2/\Delta^2 = 0.0338597$. The value used for parameter n_0^{2d} was 0.028.

5.3 Average momentum squared

We also studied the value of the gauge invariant momentum scale, given by the equation (4.2.1). The time evolution of the results for different values of parameter n_0^{2d} is shown in figure 5.4, along with the analytical prediction given by equation (4.3.19), which now simplifies to $\langle \boldsymbol{k^2} \rangle = 4\Delta^2$. We find that this prediction is in very good agreement with our results.

We can also see some non-abelian effects in figure 5.4. The values of $\boldsymbol{k^2}$ are ordered in n_0^{2d}, i.e. when we increase the value of the parameter n_0^{2d} the average momentum squared increases. This behaviour is not predicted by the abelian theory.

Interestingly, we cannot observe any time evolution for the values of the average momentum squared in the figure 5.4. We would have expected the values of the momentum scale to increase, as it has been shown that there is an UV-cascade in Yang-Mills theory ([38] , fig 1.). Briefly, this (UV-cascade) means that particles occupy states of higher and higher momentum due to the the infinite phase space available in the ultraviolet. The fact that we can not observe this might be caused by low statistics, or the fact that we have not evolved our system up to large enough dimensionless times. Yet another difference between

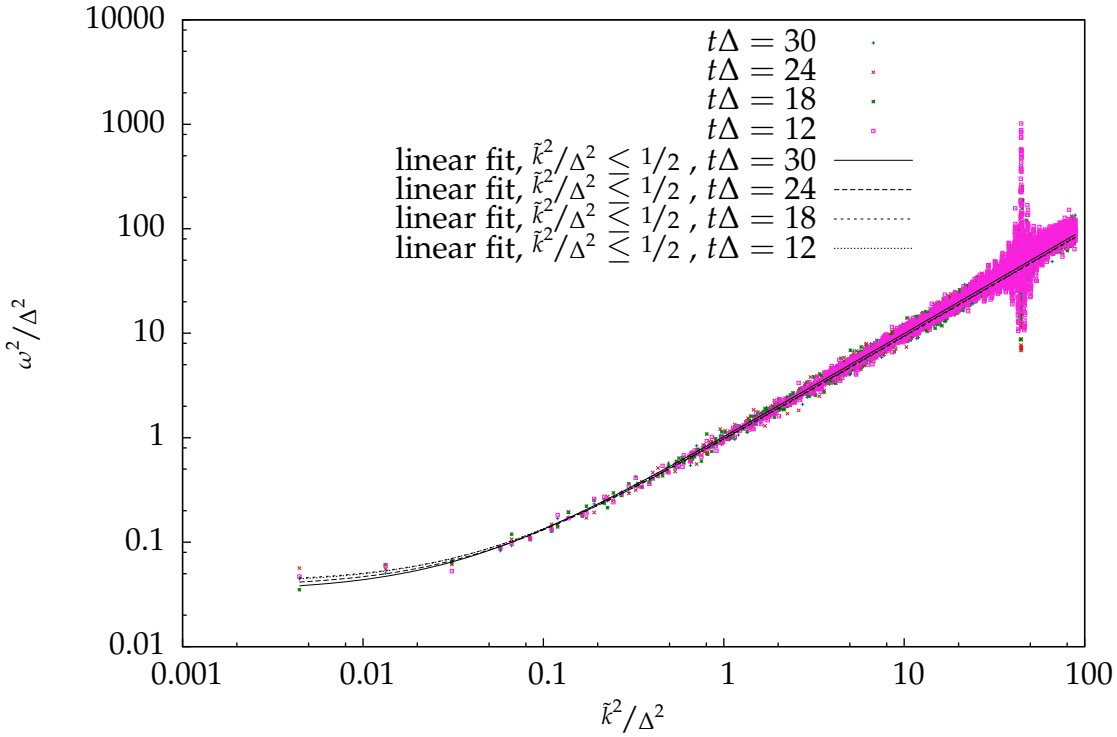

Figure 5.3: Four different dispersion relations from the same simulation at different dimensionless times. We have also performed the fits in the region in which $k^2/\Delta^2 \leq 1/2$. The value used for parameter n_0^{2d} in this simulation was 0.028.

the calculation of reference [38] and ours is that we are working with a two dimensional theory, which may affect this kind of behaviour.

5.4 Occupation number

We start studying the time-evolution of the occupation number distribution by performing a cross-check with the analytical estimate at $t = 0$ and our initial condition used in our lattice calculations. The result is shown in figure 5.5. We find that the analytical prediction and the lattice occupancy are in perfect agreement as they should be. We have also included the same distribution at $t\Delta = 30$ in the figure 5.5. We observe that the occupancy in the low momentum modes increases dramatically as time goes on.

In figures 5.6 , 5.7 and 5.8 we can see the typical time evolution of the occupation number by using the three different definitions ((4.1.10) , (4.1.11)

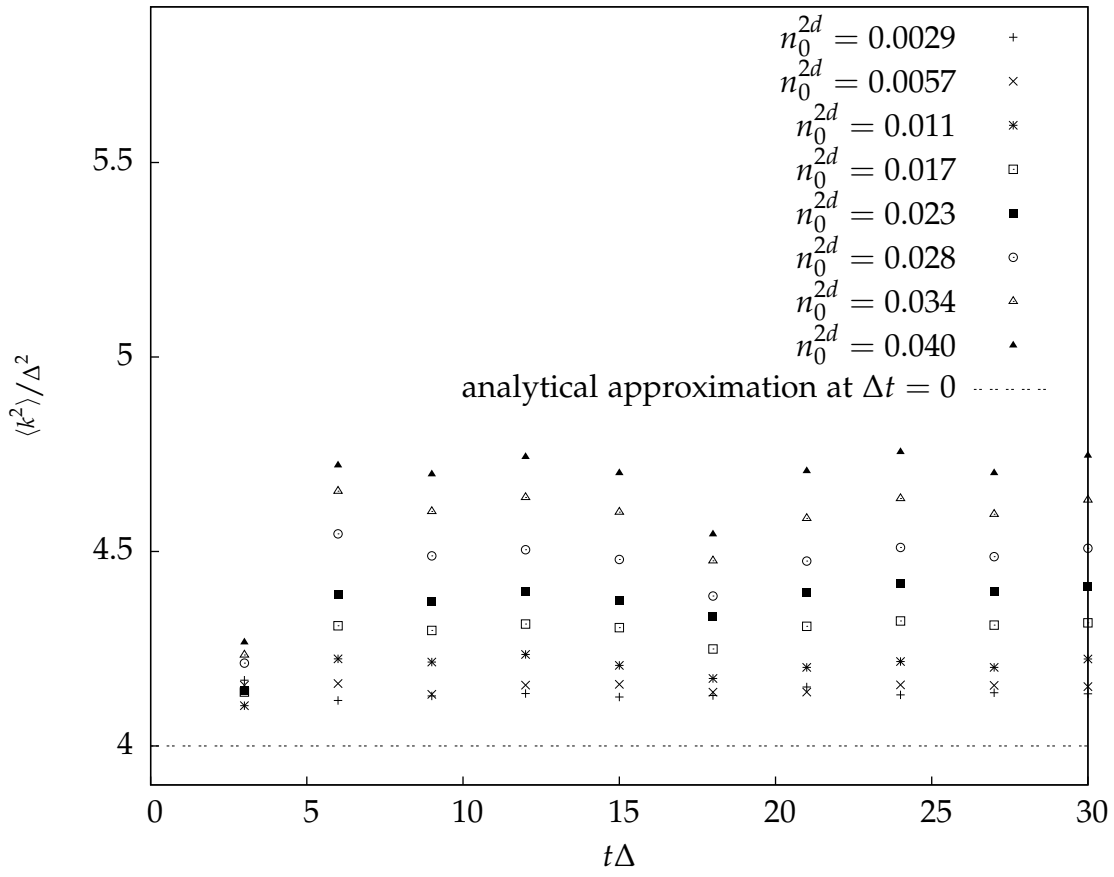

Figure 5.4: Values of momentum scale squared (calculated using (4.2.1)) for different values of Δt and n_0^{2d}.

and (4.1.12)) of the occupation number. We have also drawn the analytical estimate for the occupation number, which is given by equation (4.3.13). We find that all of these definitions predict qualitatively similar time-evolution. After initial equilibration all definitions show increased occupancy in the low momentum regime, whereas in the high momentum regime the occupation number distribution remains unchanged. We observe that particle number is not conserved, as the particle number is essentially given by the integral of the occupation number distribution. This is not a concern as we know that gluons can both fuse and split, thus we take this as an indication of gluon splitting. Figures 5.6, 5.7 and 5.8 can also be used to compare the equilibration times of different definitions of the occupation numbers. We find that n_A seems to be the most unstable definition, and n_{AE} seems to be the least unstable.

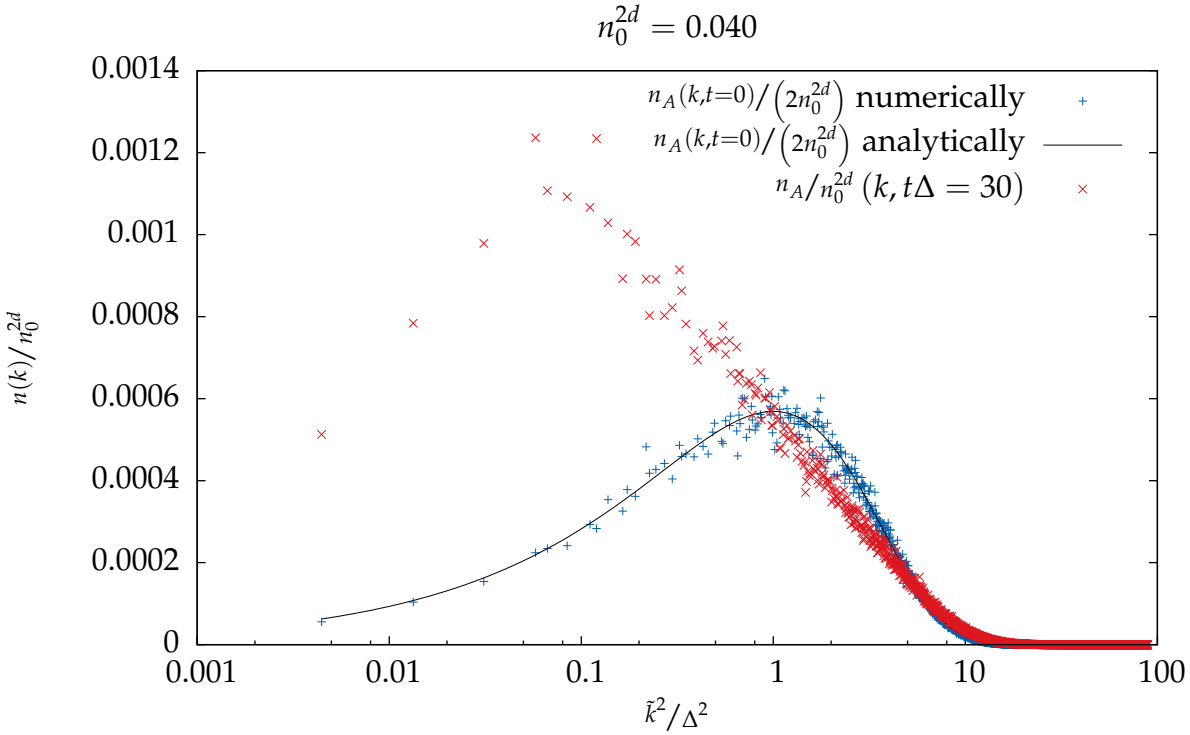

Figure 5.5: Cross-check for the occupation number distribution at $t = 0$ using equation (4.1.11) as the definition of the occupation number. We find that the analytical and numerical occupation number distributions are in excellent agreement as they should be. The $t = 0$ data has been divided by 2, because in the derivation of the different occupation number distributions we assumed that the electric and magnetic modes have approximately equal energy. This is not true for our initial condition, which contains purely magnetic energy. The solid line corresponds to an analytical calculation of the occupation number distribution using equation (4.3.13).

Figure 5.9 shows the three definitions of the occupation number at time $t\Delta = 3$. We find that these definitions are very strongly inequivalent at early times, but at late times, as shown in figure 5.10 they start to agree, except at very low momenta. Figures 5.6, 5.7 and 5.8 tell us that the occupation number distributions are oscillatory up to times $t\Delta = 18$. The initial disagreement might be due to presence of the Debye mass (which was assumed to be zero when we derived the expressions for the occupation number), or due to the fact that the system has not had enough time to equilibrate. At late times, as shown in the figure 5.10 we see that the definitions do agree, except in the low momentum regime. Here the inequivalence can be taken as an indication of the Debye mass

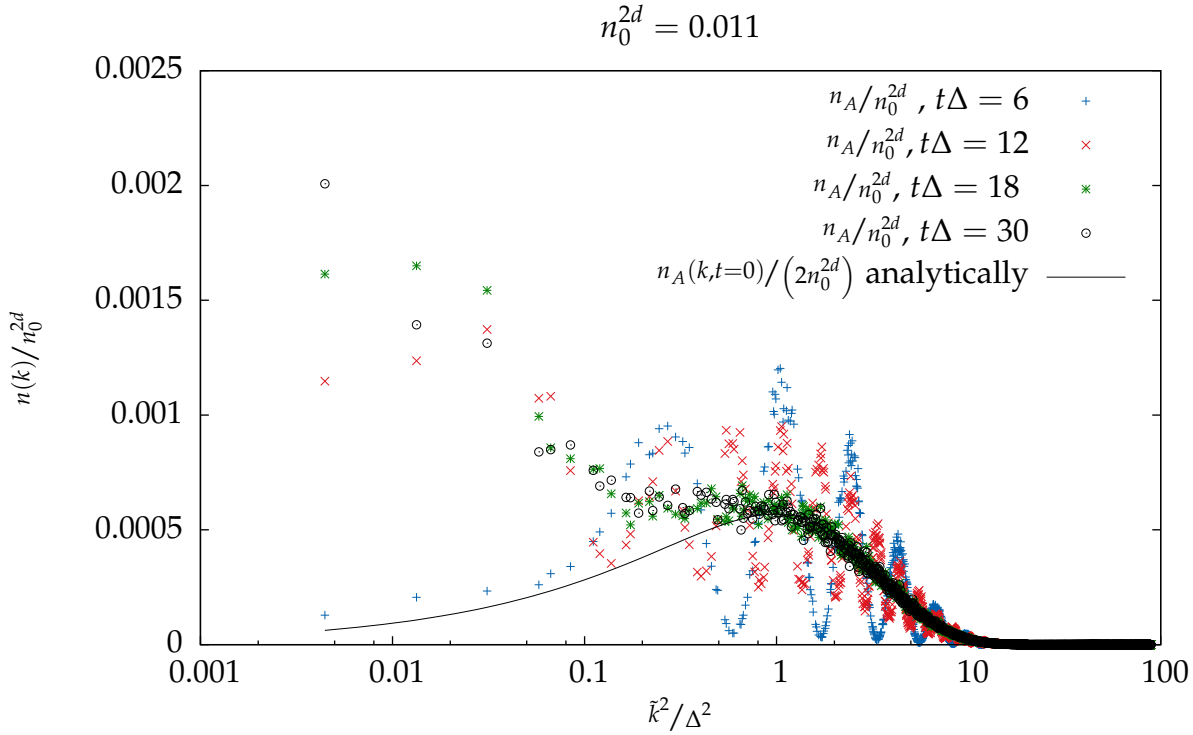

Figure 5.6: Time-evolution of the occupation number distribution using equation (4.1.11) as the definition of the occupation number. The solid line corresponds to an analytical calculation of the occupation number distribution using equation (4.3.13) divided by two to compensate the lack of elecric energy in the initial condition.

as it concerns only the low momentum regime, where the effect of the Debye mass should be visible.

The time evolution of the occupation number turns out to be interesting. Initially the distribution is heavily peaked around $k^2/\Delta^2 = 1$. Figures 5.6, 5.7 and 5.8 show that for this configuration (in which $n_0^{2d} = 0.028$) it takes around $t\Delta = 18$ for the definitions of occupation number to agree, as the oscillations are still present at $t\Delta = 12$ in all figures, but they are gone by the time $t\Delta = 18$. We do not see very much time-evolution happening between $t\Delta = 18$ and $t\Delta = 30$, which is quite interesting. This means that the value of the Debye mass should stay approximately the same according to the thermal field theory prescription, as can be seen from the equation (4.1.29). It should also be noted that there should be an UV-cascade in Yang-Mills theory, as pointed out in [38]. Our results in occupation number distributions can be compared to the ones appearing in figure 4 in [38] and in figure 1 in [34]. Both references

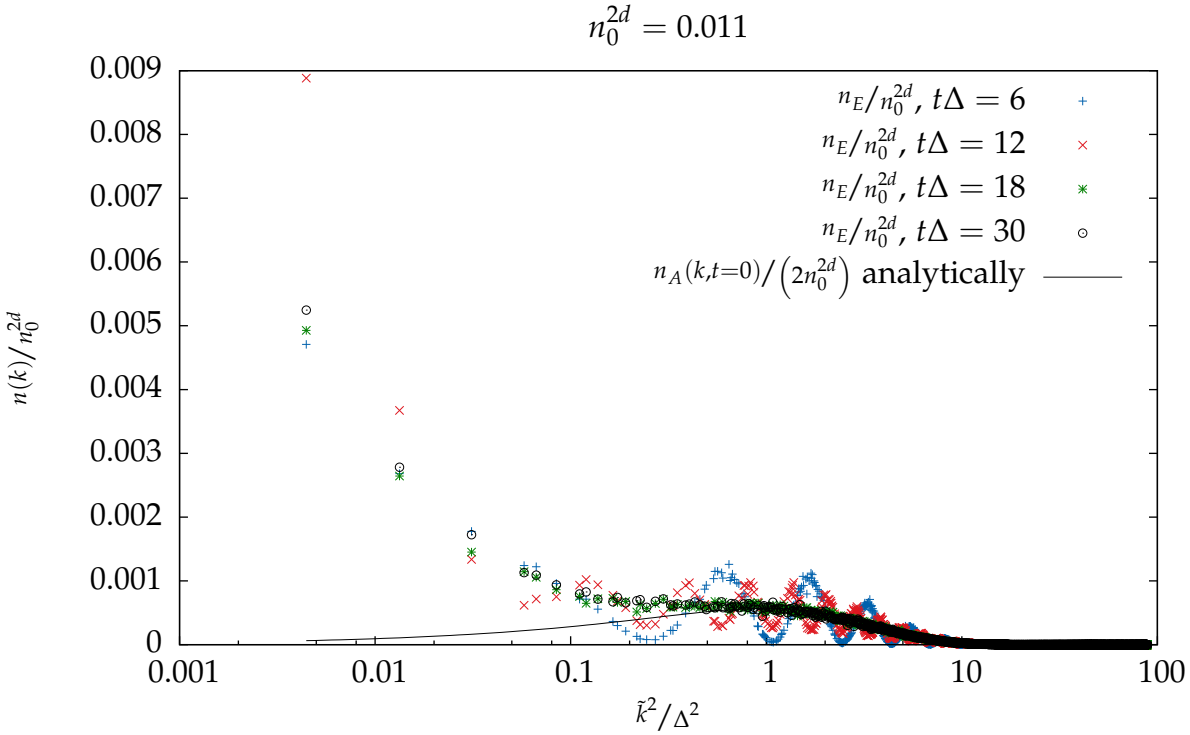

Figure 5.7: Time-evolution of the occupation number distribution using equation (4.1.12) as the definition of the occupation number. The solid line corresponds to an analytical calculation of the occupation number distribution using equation (4.3.13) divided by two to compensate the lack of elecric energy in the initial condition.

show increased occupancy in the high momentum regime, but different kind of scaling behaviour. The fact that we do not see similar scaling could be caused by the fact that we do not evolve our system so far in time and instead of full three dimensional theory we are working on two dimensional case. In reference [38] the time-evolution lasts up to thousand times longer than in our calculation. This might indicate that the reason why we can not see similar behaviour is because of insufficient time-evolution.

Figure 5.11 shows the occupation number distribution at $t\Delta = 30$ with higher occupancy. We see that now the shape of the occupation number distribution is different from the shape we saw before. Before the occupation number distribution reached a plateau-like shape in k^2 roughly at $k^2/\Delta^2 \sim 1$. Now we observe that this kind of shape has disappeared completely and has been replaced by a straigth line. The straight line corresponds to occupation number

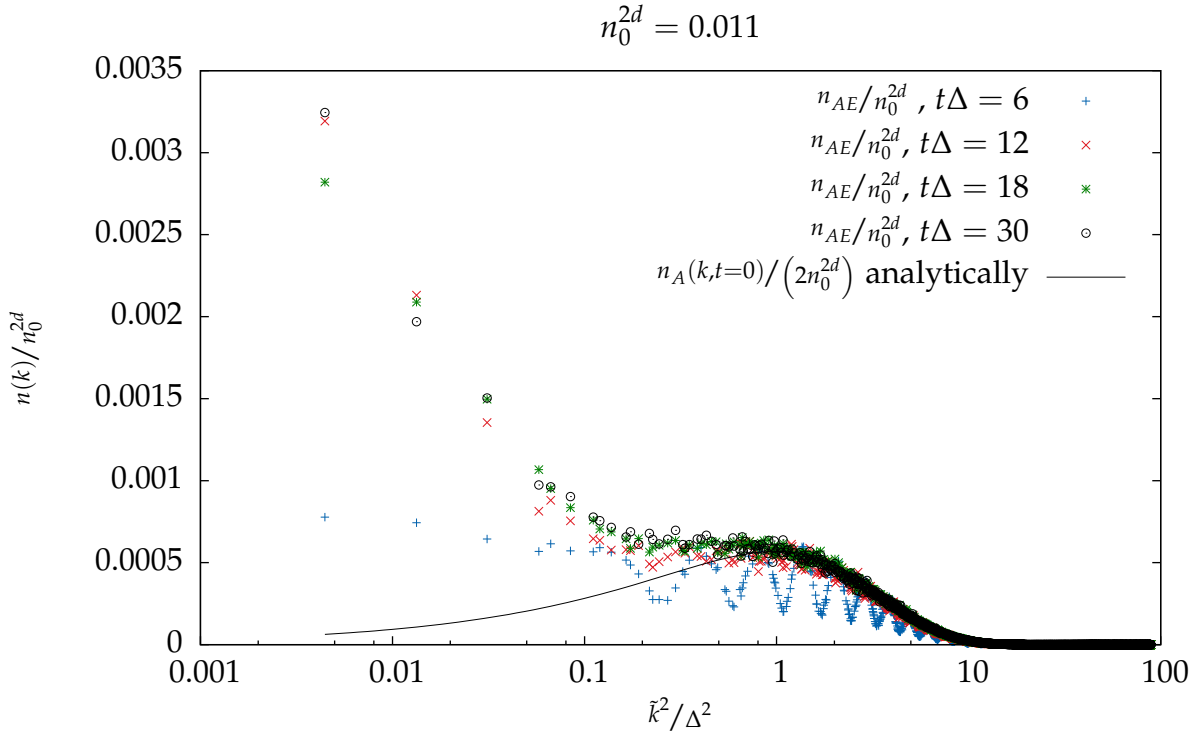

Figure 5.8: Time-evolution of the occupation number distribution using equation (4.1.10) as the definition of the occupation number. The solid line corresponds to an analytical calculation of the occupation number distribution using equation (4.3.13) divided by two to compensate the lack of elecric energy in the initial condition.

distribution in which $n \sim -\log\left(k^2\right)$. We also notice that now the equilibration time of the occupation number is considerably shorter than it was before, because even the curve at $t\Delta = 6$ in figure 5.11 does not exhibit oscillatory behaviour. This kind of behaviour is natural. In abelian theory we have no interactions, and thus the occupation number distribution is constant in time. Thus the time-evolution of our system is driven by the non-abelian interactions, which are naturally stronger at higher field amplitudes, which correspond to higher occupation numbers. Therefore we expect that similar shape of the occupation number distribution would be achieved in other simulations as well, if we evolve them far enough in time.

Interestingly, the time-evolution shown in [34] is considerably different from our time-evolution. Their initial occupation number distribution seems to be qualitatively similar to ours, which can be seen from figure one. In their

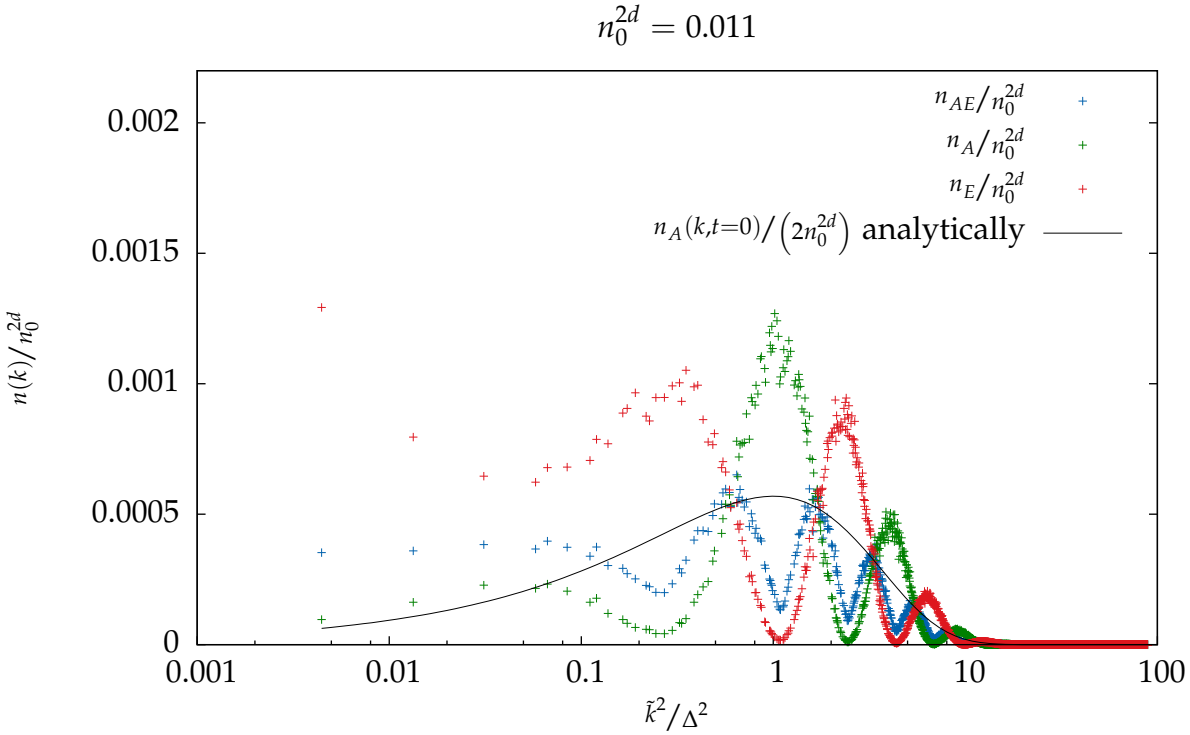

Figure 5.9: Occupation numbers calculated by using three different definitions. We see that they have some oscillatory behaviour, and that they are not yet in agreement even above the scale $k^2/\Delta^2 > 1$. We used $C = 0.011$ in this simulation. The solid line corresponds to initial (abelian) occupation number distribution, which we can calculate analytically using the definition of the occupation number involving only the gluon field (i.e. n_A) at $t\Delta = 0$.

simulation the occupation number distribution eventually reaches a power law shape, but in our simulation the occupation number distribution seems to behave as $n(k) \sim -\log\left(k^2\right)$. This remarkable difference might be caused by differences in dimensionality, but further time-evolution in two dimensions is needed to conclude that our initial condition does not evolve into a power law shape in the low momentum ($p^2/\Delta^2 < 1$) regime at asymptotically large times.

In chapter 4 we derived two expressions ((4.1.31) and (4.2.7)) for the typical occupation number of our system. The dependence of these expressions on the parameter n_0^{2d} is shown in figure 5.12. We find that both of these definitions show linear behaviour in n_0^{2d} as expected (because both energy and particle number depended linearly on n_0^{2d} in our analytical calculations in section 4.3.1),

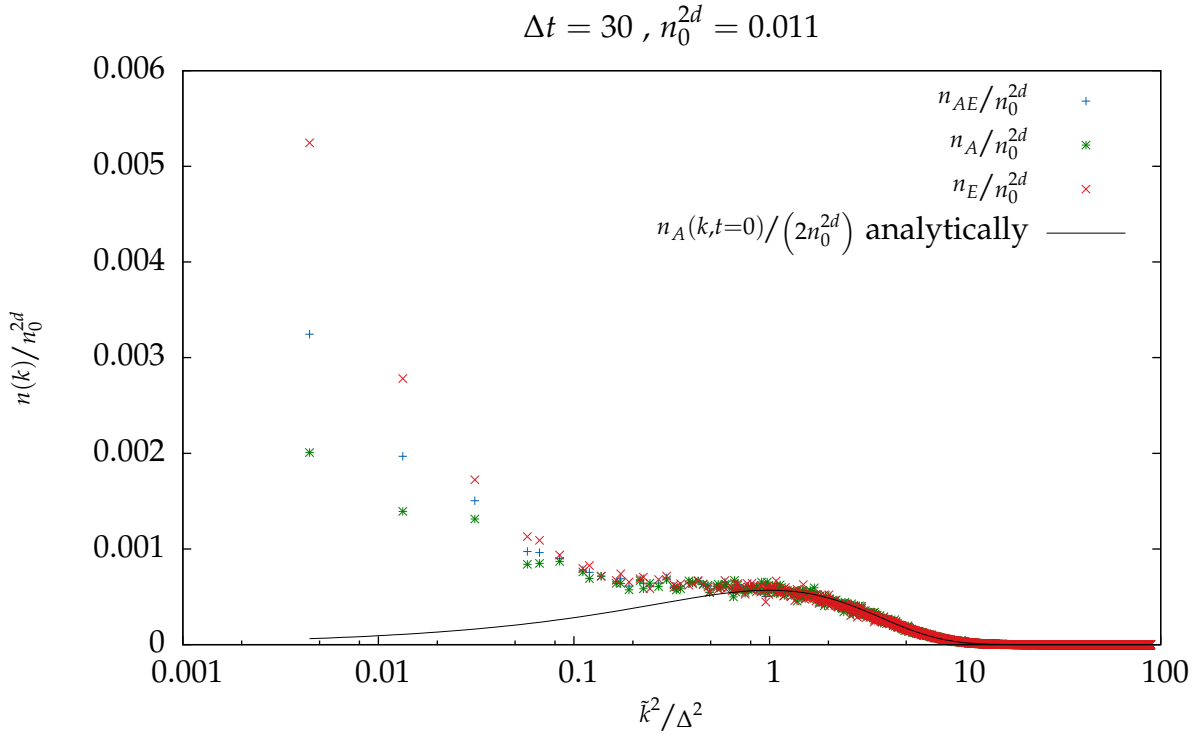

Figure 5.10: The same plot as 5.9 but at $t\Delta = 30$. Now the three definitions of the occupation number are inequivalent below $k^2/\Delta^2 \leq 0.1$, which could be caused by the existence of non-zero Debye mass. Above that scale the three definitions are in good agreement.

but the slope seems to be steeper in numerical calculations.

5.5 Energy conservation

In order to verify energy conservation we calculated the total energy of the system using two methods. First using the lattice Hamiltonian (3.1.13) and second using the dispersion relation and the equation (4.1.5) along with the numerically extracted gluon distribution function. We find that these two are in excellent agreement in the figure 5.13, which verifies that energy is indeed conserved and both approaches make sense. Values obtained using both methods have been divided by the analytical estimate for energy at $t = 0$. We find that the numerical values for energy are about 60% bigger than the ones we get by using the analytical estimate (4.3.18). It is natural that the energies obtained from the analytical estimate are smaller than the ones we

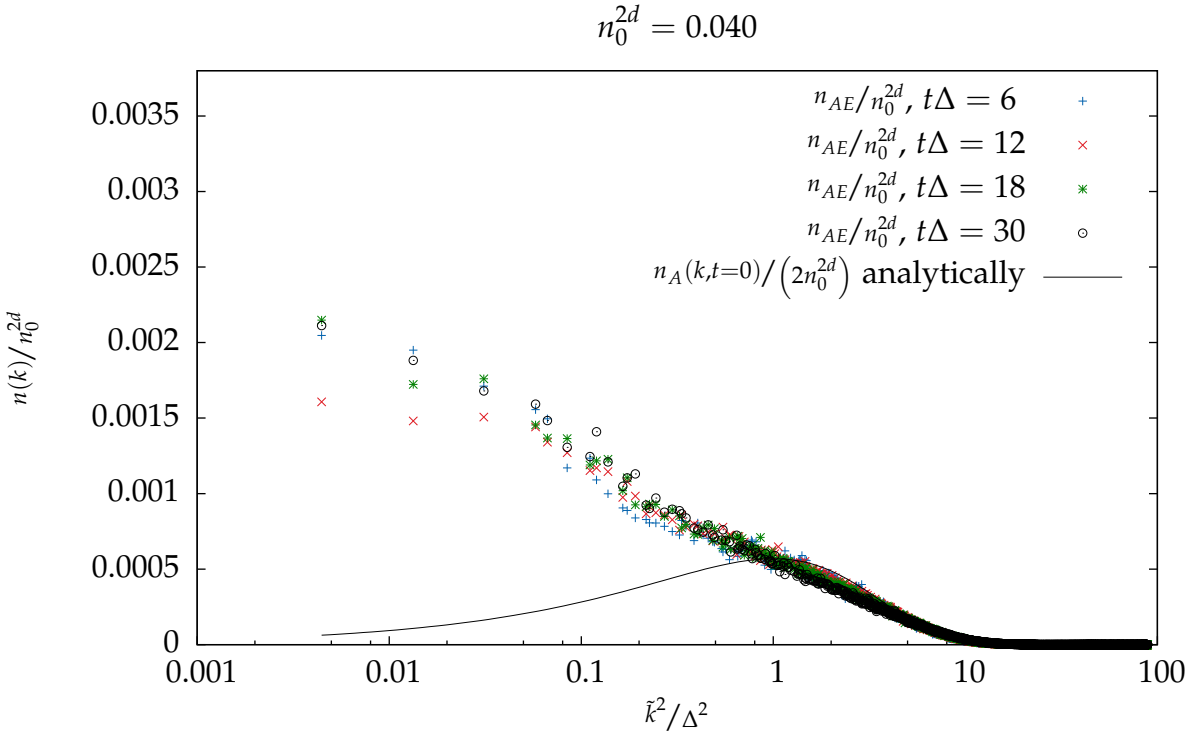

Figure 5.11: Same plot as 5.8, but now the value of the occupancy parameter n_0^{2d} used was 0.040. We can observe significantly faster time-evolution than in 5.8, due to the fact that the equilibration process is driven by the non-abelian interactions.

obtain numerically, as the analytical calculation completely omits the Debye mass. This hints that the energy stored in interactions is actually a substantial part of the total energy of the system.

Figure 5.14 shows us the division of energy between electric and magnetic modes. We find that the electric and magnetic field energies are approximately equal, and that the system tends to have very slightly more electric than magnetic energy. This verifies that the approximation we made about the equal division of energy between electric and magnetic modes is valid.

5.6 Debye screening mass

As stated in section 5.2, the values of the Debye screening mass were extracted from the data using two different methods. The first method was to perform a linear fit to the ω^2/Δ^2 vs. k^2/Δ^2 data, from which we can directly obtain the

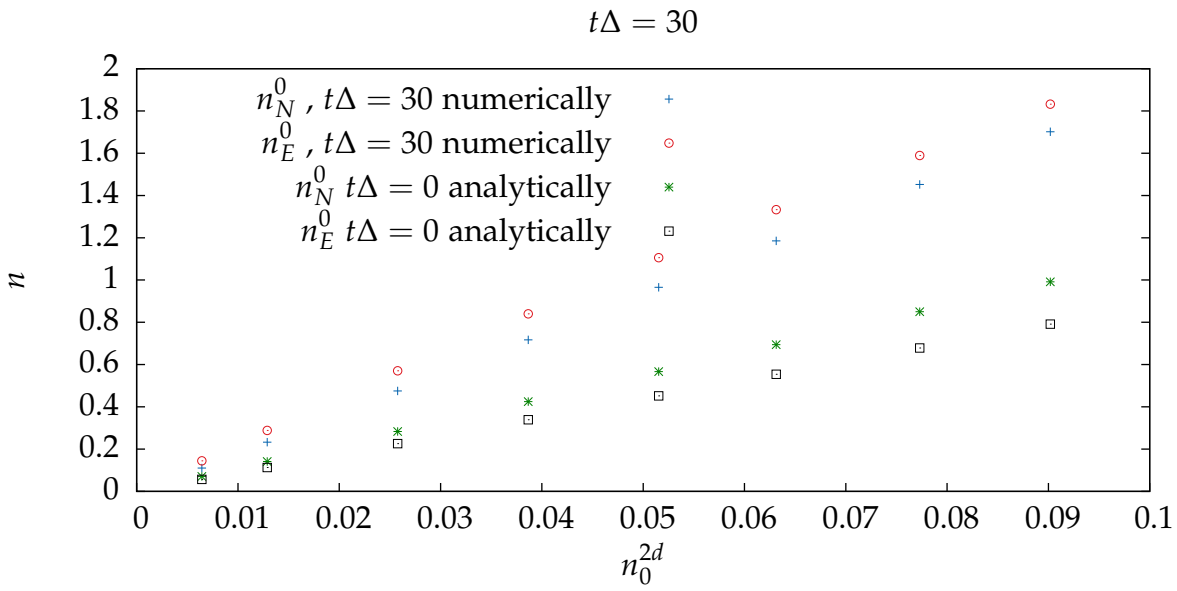

Figure 5.12: Comparison of the two different estimates for occupation number and analytic estimates for them. The steeper curves correspond to numerical calculations of n_E^0 using equation (4.2.7), and n_N^0 using equation (4.1.31). The analytical predictions have been obtained by using equations (4.3.18) for the the total energy, (4.3.16) for particle number and (4.3.19) for the gauge invariant momentum estimate. We find that the behaviour of the occupation number is linear in n_0^{2d}, but analytical approximation yields smaller results.

value of the Debye screening mass in the units of the momentum scale. The second method was using thermal field theory prescription by utilising the equation (4.1.29). We also derived the equation (4.3.20) for the Debye screening mass at $t\Delta = 0$, which can be compared to the results we obtained from our simulations.

All the fits we performed were performed to the data, in which $k^2/\Delta^2 \leq 1/2$. The values obtained were somewhat sensitive to the fit range. The fits were made with Python and Gnuplot.

As stated before, according to thermal field theory the Debye screening mass is a time dependent quantity trough the occupation number dependence as can be seen from the equation (4.1.29). From the analytical estimates, we see that the occupation of the system is dictated by the parameter n_0^{2d}. The dependence is given by equation (4.3.13) at $t = 0$.

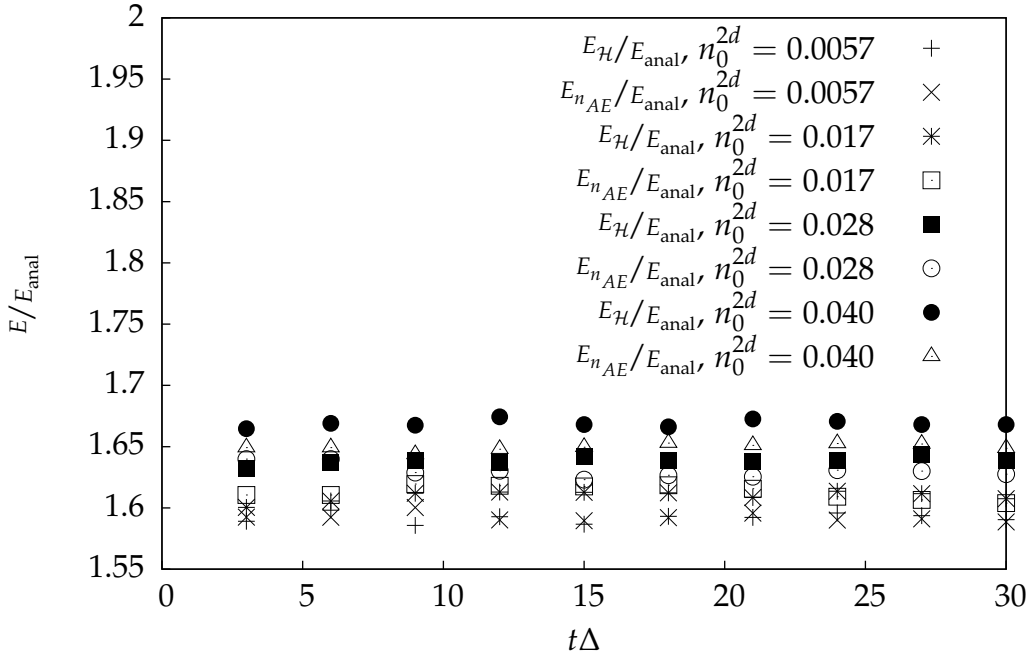

Figure 5.13: The total energy of the system calculated with different values of the parameter n_0^{2d} using two different definitions of the total energy. We find that these values are in excellent agreement.

5.6.1 Occupation number dependence

Figure 5.15 shows the dependence of the Debye screening mass in the units of the momentum scale on the parameter n_0^{2d}. We chose the late time ($t\Delta = 30$) results, because the oscillation in the dispersion relation have already died out by that time (The figure 5.1 shows that early time dispersion relation curves had huge oscillations.).

It turns out that the values we obtain from the dispersion relation grow much faster in n_0^{2d} than the values we get using the thermal field theory prescription on our lattice data using equation (4.1.29). All computations show the correct, increasing trend for the Debye mass squared in n_0^{2d}, however the thermal field theory predictions deviate considerably from the results of the fits. This might be caused by the fact, that the fits are done with quite low statistics. In order to get the dispersion relation accurately, we need data points especially at low k^2. This forces us to use very small bins, in order to access this regime. Small bins in turn lower the statistics. The effect of low statistics is visible in figure 5.15, as one Debye mass value turns out to be negative, which can not be the

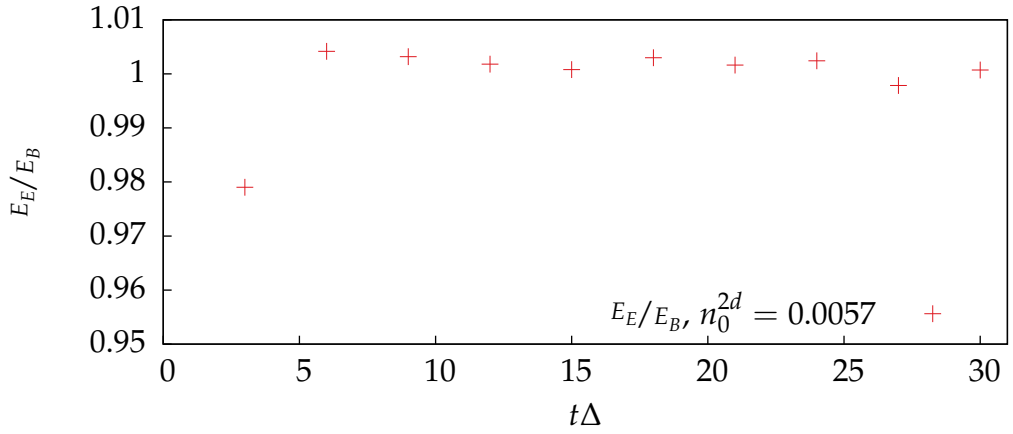

Figure 5.14: Electric total energy of the system divided by the magnetic total energy of the system for different values of $t\Delta$. The value for the occupancy parameter used was $n_0^{2d} = 0.0057$.

case. The values we get for the Debye mass are also unstable, which can be seen clearly from the figure 5.15. The Debye mass values obtained from the dispersion relation do not show consistent increase, as they also decrease at one instant. This, along with one negative value, tells us about instability and therefore we need more statistics in order to determine the values of the Debye mass accurately using the dispersion relation. However, the trend in general shows correct, increasing behaviour.

From figure 5.15 we can conclude that the values of the Debye screening mass obtained by using the thermal field theory prescription tend to increase as we increase the occupancy in our system. This means that the Debye mass behaves qualitatively as it should, when determined using thermal field theory prescription. We find that the analytical estimates using the fields at $t = 0$ and the results obtained using the thermal field theory prescription are quite consistent, even though analytical estimates yield somewhat lower values.

5.6.2 Time dependence

The time dependence of the values of the Debye screening mass is shown in the figure 5.16. We can not draw any firm conclusions on the time evolution of the Debye screening mass. The values obtained using thermal field theory prescription are almost completely constant in time, and the results from the fit show a slightly decreasing trend, but more statistics is needed to verify this. Our expectation for these results was, that the value of the Debye screening

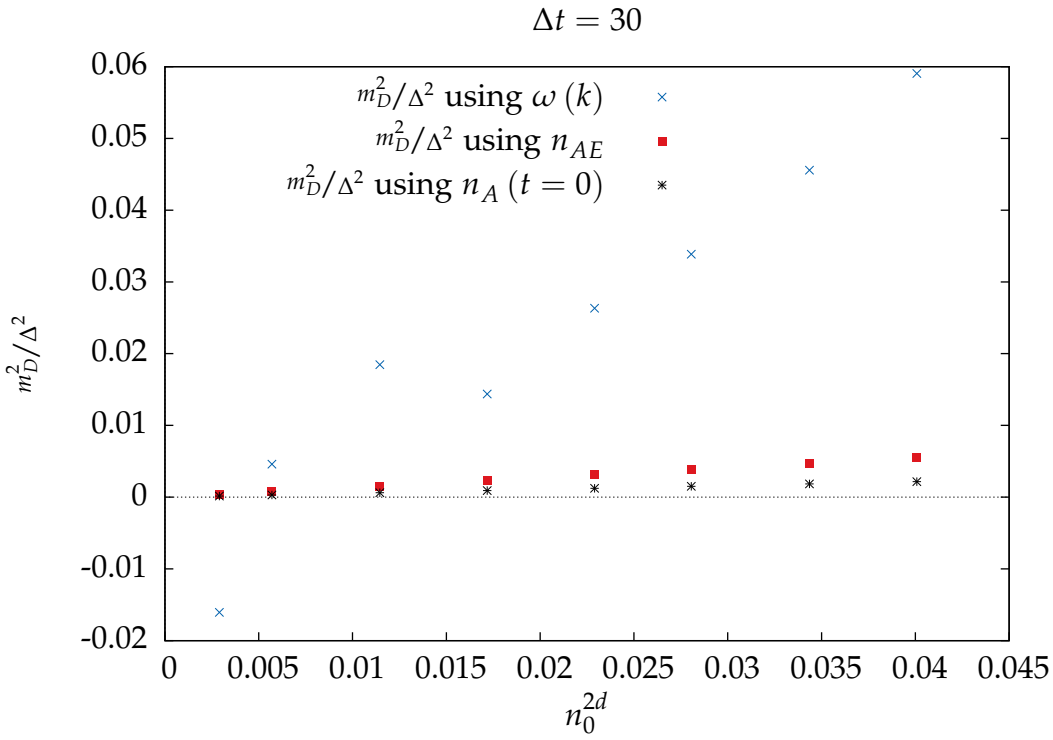

Figure 5.15: Dependence of the Debye screening mass in the units of momentum scale on the parameter n_0^{2d}. Once again values we obtained by fitting are marked in blue, and the red squares show the results we get using the thermal field theory formula (4.1.29). The values were calculated at $t\Delta = 30$.

mass should decrease in time, as such results have been obtained for example in [34] figure 3. However we should keep in mind the differences concerning dimensionality and the time-evolution of the occupation number distribution when comparing our results to those appearing in [34].

In order to get more conclusive results from the fits to the dispersion relation we will need more statics. Once again the values we get using the thermal field theory prescription are about a factor of 10 smaller than the ones we get by fitting in the small occupancy regime, and further studies are needed to shed light on this issue.

In figure 5.3 we have plotted dispersion curves of the same simulation at different times. We also show the fits to the data in the region $k^2/\Delta^2 \leq 1/2$. There we see similar behaviour as in [34], i.e. the curves are ordered in time, except for $t\Delta = 18$ and $t\Delta = 12$. The cause of this effect is probably low statistics, which causes large fitting errors. The results we get from figure 5.3 are actually the

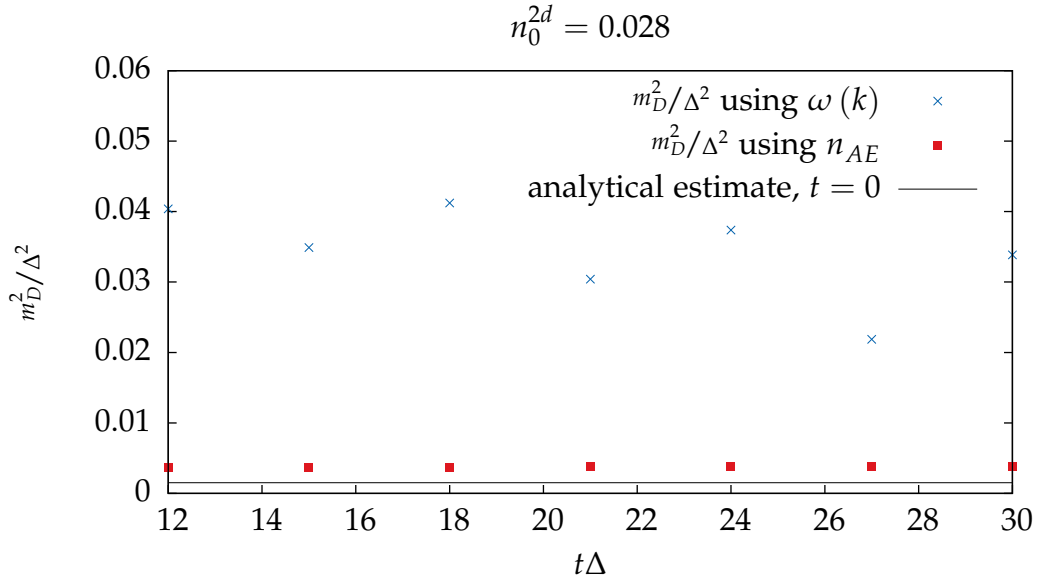

Figure 5.16: Time dependence of the Debye screening mass in the units of the momentum scale. The values of the Debye mass were obtained from the fits, which were done in the regime $k^2/\Delta^2 \leq 1/2$, are shown in blue. The red squares label the results obtained by using equation (4.1.29), predicted by the thermal field theory, on the lattice data. The definition for the occupation number used to obtain the results using the thermal field theory prescription was equation (4.1.10). We find that the values obtained using thermal field theory are a factor of ~ 10 smaller than the ones we get from the fits.

same as in figure 5.16, but here we have plotted the dispersion relation only at four different times instead of 7 in figure 5.16.

6 Conclusions

In summary we have observed a non-zero gluon Debye screening mass at sufficiently high occupation numbers. The occupation number dependence of the Debye mass seems to behave as expected by using both ways, the formula derived from thermal field theory and linear fits to the dispersion relation, to calculate the Debye mass. The thermal field theory prescription shows increased values of the Debye mass at increased occupancy. The values obtained from fits of the dispersion relation behave qualitatively similarly, but low statistics causes some instability in the fits. We could not observe any time evolution in the values of the Debye screening mass. This might be caused by low statistics, and further studies are needed to improve our results.

The values of the Debye screening mass obtained using the thermal field theory prescription, and fits to the gluon dispersion relation were not in agreement. It seems that the results obtained from the fits were a factor of 10 bigger than the results obtained from the thermal field theory prescription. The cause for this is not known, and further research is needed to shed light on the issue. Larger lattice sizes with more statistics could however yield more accurate results from the fits, which suffered considerably from low statistics in our simulations.

Interestingly, the momentum scale seems to increase as we increase the occupancy of our system. This effect is purely non-abelian, as abelian theory does not predict this kind of dependence. This does not seem to affect the values we get for the Debye screening mass, even though the increased occupancy at high momentum states should reduce its value. Thus it seems that the effect of the increased occupancy is stronger than the effect of the increased momentum scale. The momentum scale was quite close to the analytical predictions.

We could not observe any time-evolution in the momentum scale. This is interesting, because recently it has been proposed that the momentum scale should scale as $(t\Delta)^{7/2}$ [38]. Thus it would be interesting to study this further

with larger lattice sizes, more statistics and further in time. It would also be interesting to see whether the number of dimensions affect this behaviour, as our system was effectively two dimensional, whereas [38] used three dimensional system. We could also check, whether initial conditions have an impact on this issue.

We also studied the time-evolution of the occupation number distribution using three different definitions. We found that the occupation number distributions exhibit oscillatory behaviour at early times, and are also strongly inequivalent especially in the low momentum regime. At late times the occupation number distributions seemed to reach a rather steady state. After this we could not observe increase in the occupancy in the ultraviolet. This might be due to low statistics, and insufficient time-evolution.

The observed inequivalence in the definitions of the occupation numbers in the low momentum regime hints towards the existence of the Debye screening mass, as we assumed a massless dispersion relation while deriving the different expressions for the occupation number distributions. In the future it would be interesting to study the time-evolution of the occupation number distribution longer in time to see whether further time evolution occurs, and at which time scales it occurs. It has been argued that the occupation number distribution scales as $p^{-3/2}$ [34] at sufficiently high dimensionless time. It would be interesting to see whether we can find similar scaling at sufficiently high dimensionless times in three dimensions, because our two dimensional solution seems to scale as $-\log k^2$. However, to unambiguously confirm this two dimensional result, further studies are needed.

Finally we observed that we can calculate the total energy of our system using two methods. First is the field interpretation, where we calculate the total energy from the lattice Hamiltonian. And secondly by using the particle interpretation. The equivalence of these two methods tells us that we are in sufficiently weakly coupled regime for the particle interpretation to work (as particle number is not really well defined concept in interacting field theories).

In the future it would be interesting to repeat a similar study with more statistics, bigger lattice sizes and more time evolution in order to get more conclusive data on time and occupation number dependence of the Debye screening mass. An increase of factor of 10 (or even 100) in statistics should not be a problem when using a cluster, as our current simulations were done on a standard workstation lasting in total about a week. We could also take a more realistic initial condition (in the context of heavy-ion physics), which would be the McLerran-Venugopalan model [50][51][52].

Acknowledgements

I would like to thank Tuomas Lappi for instruction and insight needed to complete this work. I would also like to thank Heikki Mäntysaari for discussions and for sharing his vast Linux knowledge.

Appendices

A

Fourier transforms & Parseval theorem

A.1 Fourier transforms

We define the Fourier transform as

$$f(\boldsymbol{p}) = \int \mathrm{d}^n \boldsymbol{x} f(\boldsymbol{x}) e^{-i\boldsymbol{p}\cdot\boldsymbol{x}}. \tag{A.1.1}$$

And the inverse transform is defined as

$$f(\boldsymbol{x}) = \frac{1}{(2\pi)^n} \int \mathrm{d}^n \boldsymbol{x} f(\boldsymbol{p}) e^{i\boldsymbol{p}\cdot\boldsymbol{x}}. \tag{A.1.2}$$

We notice that if function f is real in position space, then it has hermitean symmetry in the momentum space, i.e. $f(-\boldsymbol{p}) = f(\boldsymbol{p})^\dagger$. This is easy to see by taking the complex conjugate of (A.1.1).

In discrete case the counterpart of Fourier transform is the discrete Fourier transform (DFT). Suppose we have a d dimensional array $x_{n_1,n_2,\cdots,n_d}$ with $n_l = 0, 1, \cdots, N_l - 1$. We define the DFT as

$$X_{\boldsymbol{k}} = \sum_{\boldsymbol{n}=0}^{\boldsymbol{N}-1} e^{-2\pi i \boldsymbol{k}\cdot\boldsymbol{n}/\boldsymbol{N}} x_{\boldsymbol{n}}, \tag{A.1.3}$$

where we have adopted briefer vector notation $\boldsymbol{n} = (n_1, n_2, \cdots, n_d)$, and $\boldsymbol{n}/\boldsymbol{N}$ is understood as $\boldsymbol{n}/\boldsymbol{N} = (n_1/N_1, n_2/N_2, \cdots n_d/N_d)$. The summation over $\boldsymbol{n}$ is understood as summation over all indices n_j from 0 to $N_j - 1$. Note that the result is periodic in each dimension with a period of N_j. The inverse transform is given by

$$x_{\boldsymbol{n}} = \frac{1}{\prod_{l=1}^{d} N_l} \sum_{\boldsymbol{n}=0}^{\boldsymbol{N}-1} e^{2\pi i \boldsymbol{n}\cdot\boldsymbol{k}/\boldsymbol{N}} X_{\boldsymbol{k}}. \tag{A.1.4}$$

For real data there is a similar symmetry as in continuous case. If we take each $x_{\boldsymbol{n}}$ to be real, it is easy to verify with a direct substitution that

$$X_{k_1,k_2,\cdots,k_d} = X^{\dagger}_{N_1-k_1,N_2-k_2,\cdots N_d-k_d}. \tag{A.1.5}$$

This eliminates half of the degrees of freedom of the complex data. Taking the one dimensional case as an example, it is easy to see that this symmetry is similar to the one we saw earlier in the continuous case. In one dimension we can interpret the first half of the frequencies as the positive frequencies, and the latter half as the negative frequencies in backwards order (which can be seen using periodicity). Then, similarly, in multiple dimensions the negative frequency corresponding to frequency $\boldsymbol{n}$ is the frequency $\boldsymbol{N}-\boldsymbol{n}$.

For computing purposes we can use the relation (A.1.5) to reduce the amount of storage space needed for complex data to roughly one half of the original requirement. One can use the equation (A.1.5) for the last dimension of the data, as is done by the FFTW library, to cut its size to about one half of the original. However, this does not eliminate all redundant degrees of freedom, because we are still left with some frequencies, which are real, and some are complex conjugates of others. For example the zero frequency is always real, which is quite easy to see from the equation (A.1.5). In principle it is possible to eliminate all redundant degrees of freedom in the complex data, but the implementation would be rather cumbersome.

A.2 Parseval theorem

We will go through only the magnetic contribution to the equation (4.1.7), as the electric part involves the same tricks and is easier. First we decompose the magnetic field into Fourier components and remind ourselves of the fact that in the abelian theory $\boldsymbol{B} = \boldsymbol{\nabla} \cdot \boldsymbol{A}$, and the Levi-Civita representation of the cross product. Then (4.1.7) becomes

$$\begin{aligned}\frac{1}{2}\int \mathrm{d}^3x \boldsymbol{B}^2(\boldsymbol{x}) = -\frac{1}{2}\frac{1}{(2\pi)^6}\int \mathrm{d}^3x \mathrm{d}^3k \mathrm{d}^3k' \varepsilon_{ijk}\varepsilon_{ilm}k_j A_k(\boldsymbol{k}) k'_l A_m\left(\boldsymbol{k}'\right) \\ \exp\left(i\left(\boldsymbol{k}+\boldsymbol{k}'\right)\cdot\boldsymbol{x}\right).\end{aligned}$$

Now use integral representation of the Dirac delta function, Coulomb gauge condition and the fact that $\varepsilon_{ijk}\varepsilon_{ilm} = \delta_{jl}\delta_{km} - \delta_{jm}\delta_{kl}$. We get

$$\frac{1}{2}\int \mathrm{d}^3x \boldsymbol{B}^2(\boldsymbol{x}) = -\frac{1}{2}\frac{1}{(2\pi)^3}\int \mathrm{d}^3k \mathrm{d}^3k' \left(\delta\left(k+k'\right)\boldsymbol{k}\cdot\boldsymbol{k}'\boldsymbol{A}(\boldsymbol{k})\cdot\boldsymbol{A}\left(\boldsymbol{k}'\right)\right)$$

Now use the delta function to do the integral over k' and make use of the fact that $\boldsymbol{A}(\boldsymbol{x})$ is real, therefore $\boldsymbol{A}(\boldsymbol{k}) = \boldsymbol{A}^{\dagger}(-\boldsymbol{k})$. We obtain the desired result

$$\frac{1}{2}\int \mathrm{d}^3 x \boldsymbol{B}^2(\boldsymbol{x}) = \frac{1}{2}\frac{1}{(2\pi)^3}\int \mathrm{d}^3 k \boldsymbol{k}^2 \left|\boldsymbol{A}(\boldsymbol{k})\right|.$$

B

Derivation of equation (2.2.3)

First we write (2.2.3) as,

$$\begin{aligned}\int \boldsymbol{A}^2(x)\,\mathrm{d}^3x &= \int \boldsymbol{A}(x)\cdot\boldsymbol{A}\left(x'\right)\delta\left(\boldsymbol{x}-\boldsymbol{x}'\right)\mathrm{d}^3x\mathrm{d}^3x' \\ &\equiv \int \boldsymbol{A}\cdot\boldsymbol{A}'\delta\left(\boldsymbol{x}-\boldsymbol{x}'\right)\mathrm{d}^3x\mathrm{d}^3x'.\end{aligned}$$

Now make use of the third Green's identity

$$\delta\left(\boldsymbol{x}-\boldsymbol{x}'\right) = -\frac{1}{4\pi}\boldsymbol{\nabla}^2\frac{1}{|\boldsymbol{x}-\boldsymbol{x}'|} = \frac{1}{4\pi}\boldsymbol{\nabla}\cdot\boldsymbol{\nabla}'\frac{1}{|\boldsymbol{x}-\boldsymbol{x}'|},$$

and integrate by parts (neglecting the surface terms) to get

$$\int \boldsymbol{A}^2(x)\,\mathrm{d}^3x = \frac{1}{4\pi}\int \mathrm{d}^3x\mathrm{d}^3x'\frac{\left(\boldsymbol{\nabla}\cdot\boldsymbol{\nabla}'\right)\left(\boldsymbol{A}\cdot\boldsymbol{A}'\right)}{|\boldsymbol{x}-\boldsymbol{x}'|}$$

We can write the numerator as

$$\left(\boldsymbol{\nabla}\cdot\boldsymbol{\nabla}'\right)\left(\boldsymbol{A}\cdot\boldsymbol{A}'\right) = \delta_{ii'}\delta_{jj'}\partial_i\partial'_{i'}A_jA_{j'},$$

and use

$$\varepsilon_{kij'}\varepsilon_{ki'j} = \delta_{ii'}\delta_{jj'} - \delta_{ij}\delta_{i'j'}$$

to get

$$\int \boldsymbol{A}^2\mathrm{d}^3x = \frac{1}{4\pi}\int \mathrm{d}^3x\mathrm{d}^3x'\frac{\left(\varepsilon_{kij'}\varepsilon_{ki'j}\partial'_{i'}\partial_iA'_{j'}A_j + (\boldsymbol{\nabla}\cdot\boldsymbol{A})\left(\boldsymbol{\nabla}'\cdot\boldsymbol{A}'\right)\right)}{|\boldsymbol{x}-\boldsymbol{x}'|}.$$

Now integrate by parts the term on the left hand side of the previous expression to turn the primed partial derivatives into unprimed partial derivatives and vice versa. We get

$$\frac{1}{4\pi}\int \mathrm{d}^3x\mathrm{d}^3x' \frac{(\boldsymbol{\nabla}\cdot\boldsymbol{A})\left(\boldsymbol{\nabla}'\cdot\boldsymbol{A}'\right)}{|\boldsymbol{x}-\boldsymbol{x}'|} + \frac{1}{4\pi}\int \mathrm{d}^3x\mathrm{d}^3x' \frac{\left(\varepsilon_{kij'}\partial'_i A'_{j'}\varepsilon_{ki'j}\partial_{i'}A_j\right)}{|\boldsymbol{x}-\boldsymbol{x}'|},$$

which is the desired result.

C

Exponentials of $\mathfrak{SU}(2)$ matrices

During the simulation we will also have to calculate exponentials of $\mathfrak{SU}(2)$ matrices if we are given an initial state in terms of A_μ. This can be done using the following theorem: Let $\hat{v}$ be a unit vector and $\theta \in \mathbb{R}$, then

$$\exp\left(i\theta\hat{v}\cdot\vec{\sigma}\right) = \cos\left(\theta\right)\mathbb{1} + i\sin\left(\theta\right)\hat{v}\cdot\vec{\sigma},$$

where $\vec{\sigma}$ is the Pauli vector. First we remind ourselves of the anticommutation relations of Pauli matrices $\left\{\sigma^a,\sigma^b\right\} = 2\delta^{ab}\mathbb{1}$. Then we calculate $\left(\hat{v}\cdot\vec{\sigma}\right)^2 = \mathbb{1}$. We get this result by remembering that each Pauli matrix squared is equal to one, and by using the anticommutation relations on the rest of the product. Then calculate

$$\begin{aligned}\exp\left(i\theta\hat{n}\cdot\vec{\sigma}\right) &= \sum_{n=0}^{\infty}\frac{\left(i\theta\right)^n\left(\hat{n}\cdot\vec{\sigma}\right)}{n!} = \sum_{n=0}^{\infty}\frac{\left(-1\right)^n\theta^{2n}}{(2n)!}\mathbb{1} + i\left(\hat{n}\cdot\vec{\sigma}\right)\sum_{n=0}^{\infty}\frac{\left(-1\right)^n}{(2n+1)!}\theta^{2n+1}\\ &= \cos\theta\mathbb{1} + i\sin\theta\left(\hat{n}\cdot\vec{\sigma}\right),\end{aligned}$$

where we separated the series into even and odd powers of n, made use of the powers of the Pauli vector and identified the series of sine and cosine.

By using this we can calculate exponential of an arbitrary $\mathfrak{SU}(2)$ matrix (which can be written as $\vec{v}\cdot\vec{\sigma}$, where $\vec{v}$ is a real vector with three components) expressed with normalized generators t^a, by choosing $\theta = \dfrac{||\vec{v}||}{2}$. We get

$$\exp i\vec{v}\cdot\vec{t} = \cos\left(\frac{||\vec{v}||}{2}\right)\mathbb{1} + i\sin\left(\frac{||\vec{v}||}{2}\right)\frac{2\hat{v}\cdot\vec{t}}{||\vec{v}||}.$$

D

Lattice implementation of gauge invariant momentum scale

The covariant derivative of a quantity $G_i(x)$, which transforms in a gauge transformation as $G_i(x) \to U_{x,i} G_i(x) U^\dagger_{x,i}$ can be calculated (in the direction j) as

$$D_j G_i(x) = \frac{G_i(x) - U^\dagger_{x-j,i} G_i(x-j) U_{x-j,i}}{a_s}.$$

Expanding this expression to lowest non-trivial order in lattice spacing shows that this converges to the continuum covariant derivative when lattice spacing goes to zero.

The magnetic field is calculated the using matrix form of the equation (3.1.4).

$$B_i(x) = -\frac{\varepsilon_{ijk}}{4ia_s^2 g}\left(U_{x,jk} - U^\dagger_{x,jk} - \frac{\mathbb{1}}{N}\left(U_{x,jk} - U^\dagger_{x,jk}\right)\right).$$

The cross product of covariant derivative and magnetic field can be calculated easily

$$(\boldsymbol{D} \times \boldsymbol{B})_i(x) = \varepsilon_{ijk} D_j(x) B(x)_k,$$

in which we can combine the definitions above. The squaring done in (4.2.1) can be calculated easily as the dot product of vectors whose components are matrices, and the trace is taken over the color space. The integral is easily turned into a sum, and the integration measure turns into a factor of a_s^3. Averaging was done over a range of initial conditions. In practise we calculate the integral in different simulations, and calculate the mean.

The denominator in (4.2.1) is just the total energy of the system, which is much more straightforward to calculate than the numerator.

Bibliography

[1] D. J. Gross and F. Wilczek, *Phys. Rev. Lett.* **30** (Jun, 1973) 1343.

[2] H. D. Politzer, *Phys. Rev. Lett.* **30** (Jun, 1973) 1346.

[3] D. Gross and F. Wilczek, *Phys. Rev.* **D8** (1973) 3633.

[4] H. D. Politzer, *Phys. Rept.* **14** (1974) 129.

[5] **STAR** collaboration, J. Adams *et. al.*, *Nucl. Phys.* **A757** (2005) 102 [arXiv:nucl-ex/0501009 [nucl-ex]].

[6] **BRAHMS** collaboration, I. Arsene *et. al.*, *Nucl. Phys.* **A757** (2005) 1 [arXiv:nucl-ex/0410020 [nucl-ex]].

[7] **PHENIX** collaboration, K. Adcox *et. al.*, *Nucl. Phys.* **A757** (2005) 184 [arXiv:nucl-ex/0410003 [nucl-ex]].

[8] B. Back, M. Baker, M. Ballintijn, D. Barton, B. Becker *et. al.*, *Nucl. Phys.* **A757** (2005) 28 [arXiv:nucl-ex/0410022 [nucl-ex]].

[9] **ALICE** collaboration, K. Aamodt *et. al.*, *Phys. Rev. Lett.* **105** (2010) 252302 [arXiv:1011.3914 [nucl-ex]].

[10] **ALICE** collaboration, K. Aamodt *et. al.*, *Phys. Lett.* **B696** (2011) 30 [arXiv:1012.1004 [nucl-ex]].

[11] **ALICE** collaboration, K. Aamodt *et. al.*, *Phys. Rev. Lett.* **106** (2011) 032301 [arXiv:1012.1657 [nucl-ex]].

[12] **ATLAS** collaboration, G. Aad *et. al.*, *Phys. Rev. Lett.* **105** (2010) 252303 [arXiv:1011.6182 [hep-ex]].

[13] **CMS** collaboration, S. Chatrchyan *et. al.*, *Phys. Rev.* **C84** (2011) 024906 [arXiv:1102.1957 [nucl-ex]].

[14] P. Huovinen, arXiv:nucl-th/0305064 [nucl-th].

[15] P. Kolb, P. Huovinen, U. W. Heinz and H. Heiselberg, *Phys. Lett.* **B500** (2001) 232 [arXiv:hep-ph/0012137 [hep-ph]].

[16] T. Hirano, U. W. Heinz, D. Kharzeev, R. Lacey and Y. Nara, *Phys. Lett.* **B636** (2006) 299 [arXiv:nucl-th/0511046 [nucl-th]].

[17] J. Casalderrey-Solana, H. Liu, D. Mateos, K. Rajagopal and U. A. Wiedemann, arXiv:1101.0618 [hep-th].

[18] V. Balasubramanian, A. Bernamonti, J. de Boer, N. Copland, B. Craps *et. al.*, *Phys. Rev.* **D84** (2011) 026010 [arXiv:1103.2683 [hep-th]].

[19] E. Iancu and R. Venugopalan, arXiv:hep-ph/0303204 [hep-ph].

[20] F. Gelis, E. Iancu, J. Jalilian-Marian and R. Venugopalan, *Ann. Rev. Nucl. Part. Sci.* **60** (2010) 463 [arXiv:1002.0333 [hep-ph]].

[21] F. Gelis, T. Lappi and R. Venugopalan, *Int. J. Mod. Phys.* **E16** (2007) 2595 [arXiv:0708.0047 [hep-ph]].

[22] J. Berges, K. Boguslavski, S. Schlichting and R. Venugopalan, arXiv:1311.3005 [hep-ph].

[23] T. Lappi, *Phys. Rev.* **C67** (2003) 054903 [arXiv:hep-ph/0303076 [hep-ph]].

[24] K. G. Wilson, *Phys. Rev. D* **10** (Oct, 1974) 2445.

[25] E. S. Weibel, *Phys. Rev. Lett.* **2** (1959) 83.

[26] M. Strickland, *J. Phys.* **G34** (2007) S429 [arXiv:hep-ph/0701238 [HEP-PH]].

[27] N. Nielsen and P. Olesen, *Nucl. Phys.* **B144** (1978) 376.

[28] D. Mateos and D. Trancanelli, *JHEP* **1107** (2011) 054 [arXiv:1106.1637 [hep-th]].

[29] P. B. Arnold, J. Lenaghan, G. D. Moore and L. G. Yaffe, *Phys. Rev. Lett.* **94** (2005) 072302 [arXiv:nucl-th/0409068 [nucl-th]].

[30] P. Romatschke and R. Venugopalan, *Phys. Rev. Lett.* **96** (2006) 062302 [arXiv:hep-ph/0510121 [hep-ph]].

[31] J. I. Kapusta, *Finite-Temperature field theory*. 1989.

[32] J. Berges, S. Scheffler and D. Sexty, *Phys. Rev.* **D77** (2008) 034504 [arXiv:0712.3514 [hep-ph]].

[33] J. Berges, D. Gelfand, S. Scheffler and D. Sexty, *Phys. Lett.* **B677** (2009) 210 [arXiv:0812.3859 [hep-ph]].

[34] J. Berges, S. Schlichting and D. Sexty, *Phys. Rev.* **D86** (2012) 074006 [arXiv:1203.4646 [hep-ph]].

[35] S. Jeon, *Phys. Rev.* **C72** (2005) 014907 [arXiv:hep-ph/0412121 [hep-ph]].

[36] A. Mueller and D. Son, *Phys. Lett.* **B582** (2004) 279 [arXiv:hep-ph/0212198 [hep-ph]].

[37] M. C. A. York, A. Kurkela, E. Lu and G. D. Moore, *Phys. Rev.* **D89** (2014) 074036 [arXiv:1401.3751 [hep-ph]].

[38] A. Kurkela and G. D. Moore, *Phys. Rev.* **D86** (2012) 056008 [arXiv:1207.1663 [hep-ph]].

[39] C.-N. Yang and R. L. Mills, *Phys. Rev.* **96** (1954) 191.

[40] V. Gribov, *Nucl. Phys.* **B139** (1978) 1.

[41] F. Gubarev, L. Stodolsky and V. I. Zakharov, *Phys. Rev. Lett.* **86** (2001) 2220 [arXiv:hep-ph/0010057 [hep-ph]].

[42] C. Davies, G. Batrouni, G. Katz, A. S. Kronfeld, G. Lepage *et. al.*, *Phys. Rev.* **D37** (1988) 1581.

[43] F. Karsch, *Lect. Notes Phys.* **583** (2002) 209 [arXiv:hep-lat/0106019 [hep-lat]].

[44] R. Gupta, arXiv:hep-lat/9807028 [hep-lat].

[45] A. Ipp, A. Rebhan and M. Strickland, *Phys.Rev.* **D84** (2011) 056003 [arXiv:1012.0298 [hep-ph]].

[46] M. Frigo and S. G. Johnson, *Proceedings of the IEEE* **93** (2005)no. 2 216. Special issue on "Program Generation, Optimization, and Platform Adaptation".

[47] N. Stamatopoulos, arXiv:1201.3368 [hep-th].

[48] D. Bodeker and K. Rummukainen, *JHEP* **0707** (2007) 022 [arXiv:0705.0180 [hep-ph]].

[49] R. Baier, A. H. Mueller, D. Schiff and D. Son, *Phys. Lett.* **B502** (2001) 51 [arXiv:hep-ph/0009237 [hep-ph]].

[50] L. D. McLerran and R. Venugopalan, *Phys. Rev.* **D49** (1994) 2233 [arXiv:hep-ph/9309289 [hep-ph]].

[51] L. D. McLerran and R. Venugopalan, *Phys. Rev.* **D49** (1994) 3352 [arXiv:hep-ph/9311205 [hep-ph]].

[52] L. D. McLerran and R. Venugopalan, *Phys. Rev.* **D50** (1994) 2225 [arXiv:hep-ph/9402335 [hep-ph]].